Building 3-D Crustal Model with Radial Anisotropy in Iceland from Ambient Seismic Noise Tomography

---

A Thesis

Presented to

The Faculty of the Department of Earth and Atmospheric Sciences

University of Houston

In Partial Fulfillment

of the Requirements for the Degree

Master of Science

By

Duo Yuan

May 2013

Building 3-D Crustal Model with Radial Anisotropy in Iceland from Ambient Seismic Noise Tomography

Duo Yuan

APPROVED:

_____

Dr. Aibing Li

_____

Dr. Jonathan Snow

_____

Dr. Dale Bird

_____

Dean, College of Natural Sciences and Mathematics

Acknowledgments

First and foremost, I would like to express my appreciation to my advisor, Dr Aibing Li, for her support during my MS study and research in the geophysics area. Dr Li introduced me to a brand new field since I had no geophysical background. She also gives me encouragement, assistance, and inspiration in many aspects. Without her help, I would not have been so happy to be in this field and learn so much. Then I would like to give my appreciation to Dr Snow and Dr Bird, who brought me many thoughts. I would also like to thank Lu Li and Dr Yuanyuan Fu, who helped me a lot for data processing.

I would also give my sincerely gratitude to SEG for financial support, without which my MS study and research would not have been so smooth.

In the end, I would like to give my thanks to my parents and my girlfriend, Xuexi Gu, for all the support they gave me.

ABSTRACT

Iceland is a place of great geophysical interest due to its location at a hotspot and on the Mid-North Atlantic Ridge. Despite numerous studies conducted on Iceland, there remain fundamental disagreements on such questions as whether the Icelandic crust is thin or thick, cold or hot. In addition, crustal seismic anisotropy, which can be caused by strain-induced preferred orientation of cracks, melt pockets, or crustal minerals, has not been well studied in Iceland. To improve our understanding of crustal formation and evolution of Iceland, Love wave tomography was conducted using ambient noise data recorded at the HOTSPOT experiment, which consists of 30 broadband seismic stations and operated from June of 1996 to August of 1998. Love wave phase velocity maps from 6 to 40 s were obtained. Then the phase velocities were inverted for 1D and 3D isotropic SH wave velocity in Iceland. The low velocity anomaly in shallow crust can be found along ridge and major volcanic zones which would probably be associated with partial melt that feeds the volcanoes, while low velocities is near the hotspot at deep crust, indicating melt accumulation or high temperature from the Iceland plume. Finally, the isotropic V_{SH} model from Love wave inversion was combined with existing V_{SV} model from previous Rayleigh wave study to establish a 3-D radial anisotropic model. In upper crust, $V_{SV}>V_{SH}$ is largely found in the rifting zones, reflecting vertical alignment of cracks and melt sills. This finding suggests that horizontal flow that feeds mid-ocean

ridges from the plume source is not strong in the upper crust of Iceland. In the lower crust, $V_{SV}>V_{SH}$ concentrates at the current hotspot location while $V_{SH}>V_{SV}$ occurs everywhere else in Iceland. This observation can be interpreted as vertical flow beneath the mantle plume and horizontal flow that transports crustal materials from the plume center to other rift zones in Iceland, suggesting that melt produced from the mantle plume is the dominant source for forming the crust of Iceland.

Table of Contents

Chapter 1 Introduction

1.1 Background and motivation

Iceland sits astride the Mid-Atlantic ridge, a plate boundary between the actively separating North American plate and Eurasian plate. Tensional forces fracture the crust, mantle melts and subsequent magma intrude to form new ocean crust. Meanwhile, it is generally agreed that Iceland is underlain by a hot mantle plume that is located beneath the central and northwestern Vatnajokull Icecap in southeastern Iceland, making it one of the best natural laboratories for studying plume-ridge interaction (Figure 1). The Mid-Atlantic Ridge extends for about 16,000 km in a curving path from the Arctic Ocean to near the southern tip of Africa. Most part of the ridge is submarine except for Iceland. The transverse ridge is asymmetric about Iceland where the southern ridge appears to have jumped from a more westward location to a more eastward location across the current Iceland hotspot.

Due to its unique tectonic setting, Iceland contains several active rift zones and volcanic areas (Figure 1 and 2). In south Iceland, the spreading occurs at the Western and Eastern Volcanic Zones (WVZ, EVZ). In northern part of Iceland, spreading place only consists of the Northern Volcanic Zones (NVZ). And all these Volcanic Zones are connected by the Middle Volcanic Zone (MVZ).

Along the EVZ and NVZ, there are five major volcanic complexes, which are Katla, Hekla, Bardarbunga, Grimsvotn, Askja, and Krafla, from south to north.

There are two big glaciers in Iceland, called Vatnajokull and Hofs in the EVZ and MVZ, respectively. In the last 20 million years Iceland's rift zones have moved stepwise to the east in order to keep their positions next to the surface expression of the hot spot. This process leads to a complex and shifting pattern of local rift zones and transform fault zones.

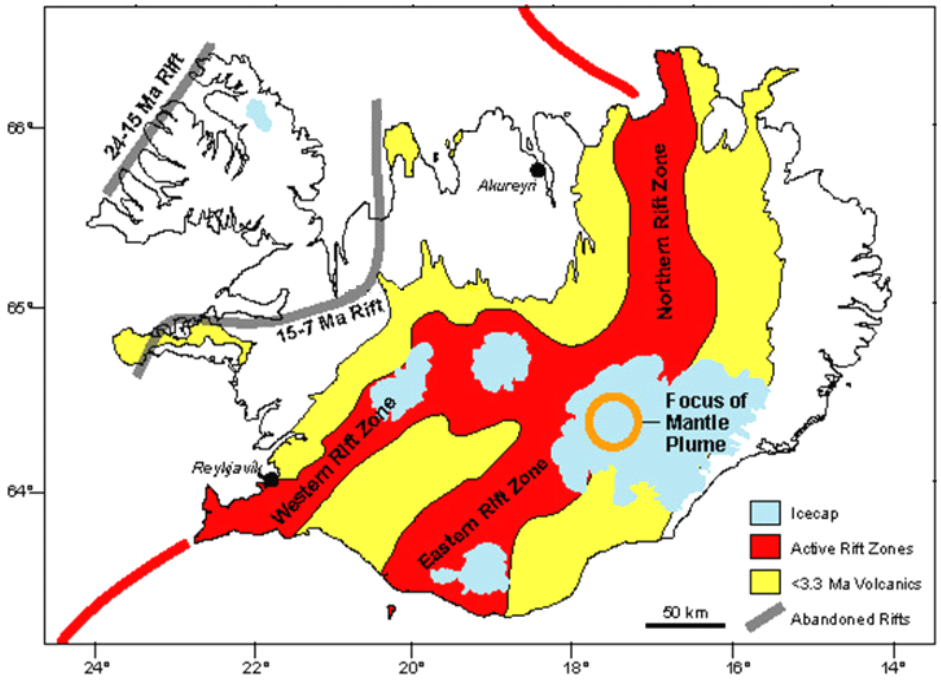

Figure 1 *Maps of active rift zones and the location of mantle plume in Iceland. It also shows the jump of rift during 20 million years. [Image from the Iceland 2003 Keck Consortium Project]*

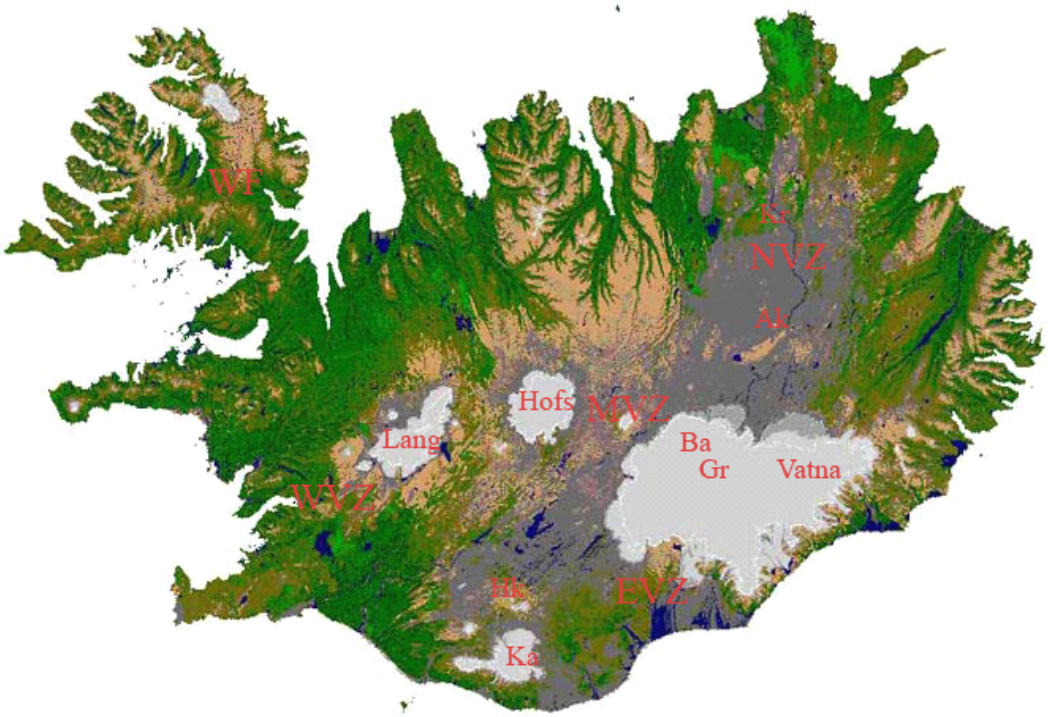

Figure 2 *Location map of the volcanoes, glaciers and tectonic features mentioned in this paper (Ak Askja volcano; Ba Bardarbunga volcano; Gr Grimsvotn volcano; Hk Hekla volcano; Kr Krafla volcano; WF Westernfjords; Hofs Hofsjokull glaciers; Lang Langjokull glaciers; Vatna Vatnajokull glaciers; NVZ Northern Volcanic Zone; EVZ Eastern Volcanic Zone; WVZ Western Volcanic Zone; MVZ Middle Volcanic Zone).*

What also makes Iceland unique is its crustal structure. The typical thickness of oceanic crust is 6-7 km and is remarkably similar around the world. In contrast, continental crust is more complex and with a typical thickness of 35-45 km. However,

the crust of Iceland differs from typical oceanic crust with an average depth of 29km [Allen *et al.*, 2002]. Bott [1974] proposed a new term, Icelandic-type crust, and pointed out that the generation of each layer of the Icelandic crust is the same as normal oceanic crust.

Bath [1960] conducted the pioneer of geophysical study in Iceland by measuring explosion seismic profiles. Since then numerous studies have been done using almost all kinds of geophysical methods to build crust and mantle models beneath Iceland. In the last four decades, the assumption that Iceland is underlain by a hot mantle plume has great effect on the Icelandic-type crust studies. The crustal model in Iceland has evolved from a thin-hot model [Tryggvason, 1962; Palmason, 1971] to a thick-cold model [Bath, 1960] then to a thick-hot type of model [Allen *et al.*, 2002]. Details of these previous models are reviewed in next section of this thesis. The thin-hot model is basically abandoned due to new evidence for thick crust in Iceland. However, whether the Iceland crust is cold or hot and how the formation of the Iceland crust is affected by the mantle plume are debatable questions.

One way to investigate plume-ridge interaction in Iceland crust is to map crustal flow pattern. Crustal seismic anisotropy is a powerful tool to reveal alignment of cracks, melt sills, and general crustal material that reflects crustal strain distribution and flow direction. It helps to understand dynamic magma movement in this region and the crustal deformation in Iceland. Despite its importance, seismic anisotropy in the crust of Iceland is poorly determined.

Here I present the results of a fully 3-D shear wave model of Icelandic crustal structure including radial anisotropy. The new model was developed by combining ambient noise Love wave tomography from this study with previous obtained Rayleigh wave tomography in Iceland. First, ambient noise data acquired in the HOTSPOT experiment were processed at periods of 6-35 s and were used to determine Love wave phase velocities maps. Then these phase velocity maps at periods of 6-25s are taken as input to 3-D isotropic shear wave inversion to construct a 3D isotropic SH wave model. Finally, a crustal radial anisotropy model was developed using both Love wave phase velocities from this study and Rayleigh wave dispersion maps from a previous study . The anisotropic crustal model sheds new light on crustal formation of Iceland and provides new evidence for plume-ridge interaction.

The outline of this paper is as follows. In chapter 2, I review three typical crustal models in Iceland, the thick-cold model, thin-hot model, and thick-hot model, and other previous studies that have great influence on the crustal structure of Iceland. Data analysis, the method of ambient noise tomography is presented in chapter 3. The results of Love wave tomography are presented in chapter 4. The 1-D and 3-D shear wave models and radial anisotropy model are showed in chapter 5. Interesting features of the models and their implication for the formation and evolution of Icelandic crust are discussed in chapter 6.

Chapter 2 Previous studies

2.1 Famous typical crustal models in Iceland

2.1.1 The thin-hot crustal model

In 1962, Tryggvason got Raylaigh and Love wave dispersion curves from 20 earthquakes and interpreted them with a three-layered model. He also found a high velocity layer with a Vp of 7.4 km/s, however, in his model, this was considered to be upper mantle. There is only a 10 km crust that lies above the mantle in Iceland in his model. Ten years later, Palmason [1971] gathered data on 40 profiles that cover almost the whole of Iceland and used traditional seismic refraction methods for data processing. What he concluded is almost the same as Tryggvason [1962], that the crust in Iceland is hot and thin. He also emphasized the lateral heterogeneity of the Icelandic crust and developed a layered model involving average velocities and interface depth ranges. In 1973 Palmason observed a high temperature gradient in a near-surface borehole, which supported his thin-hot crustal model to some extent. There models are shown in Figure 3 (b) and (c).

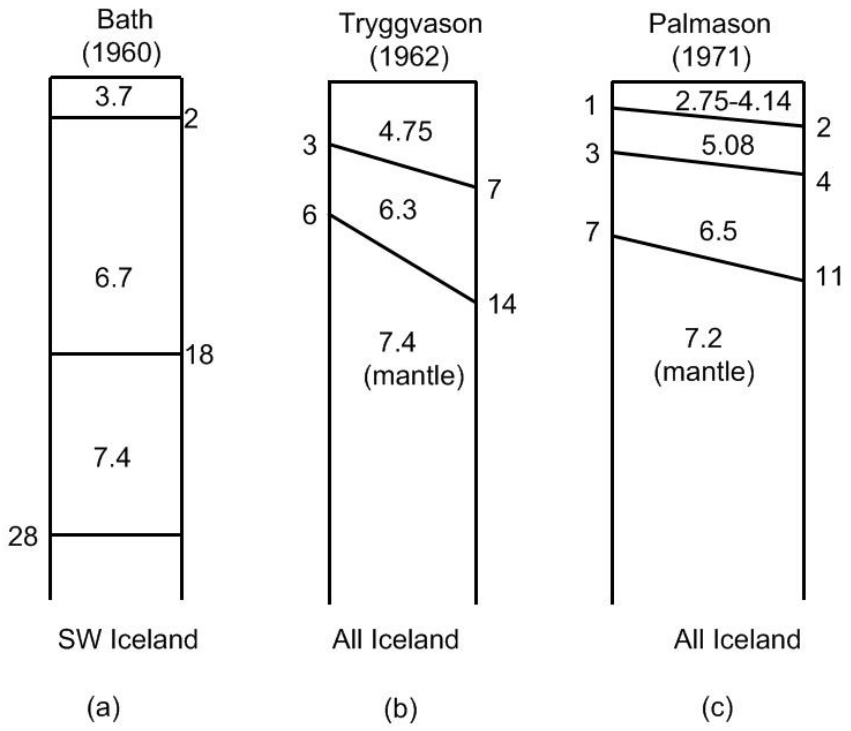

Figure 3 *Models of seismic crustal structure from early explosion and earthquake surface wave experiments. (a) is thick-cold-crustal model. (b) and (c) are thin-hot-crustal models.*

The thin-hot crustal model dominated Icelandic-type crust interpretation since it was introduced in the 1970s until the 1990s. Numerous studies were interpreted with this model [Flovenz, 1980; Gebrande *et al.*, 1980]. However, this model was challenged by early study from seismic exploration [Bath, 1960] and more studies in 1990s. The Moho depth was placed at 20-24 km from a study of PmP reflections along a 2-D seismic line in southwestern Iceland. [Bjarnason *et al.*, 1993]. Most relatively recent studies placed the crust depth between 15 km and 43 km. [Staples *et al.*, 1997; Darbyshire *et al.*, 1998] The thin-hot crustal model gradually

was abandoned and a thick-cold crustal model started to be prevalent of interpretation of Icelandic type crust.

2.1.2 The thick-cold crustal model

In the past few decades, Iceland has attracted attention of numerous geophysicists who have conducted a series of important studies on Iceland crustal structure. Early seismological studies of the crust beneath the Iceland transverse ridge used P-phase arrival times. Bath [1960] utilized the conventional 2D long profile seismic reflection survey to constrain the structure of the upper crust and provide information about the deeper crust and depth to the Moho. Two unreversed explosion profiles, with 150km in western Iceland and 250km in central Iceland, are used in his study. He derived a simple three-layered constant velocity model to interpret the times of first arrivals and a high velocity lowest layer with Vp 7.4km/s was attributed to crust. This is the early thick-cold-crustal model of Iceland. This model is shown in Figure 3 (a).

Bjarnason *et al.* [1993] conducted a seismic survey of 170km starting from the west coast of Iceland across Western Volcanic Zones (WVZ), Eastern Volcanic Zones(EVZ), and South Iceland Seismic Zones (SISZ). Using high-resolution tomography. They concluded that the depth of the Moho is around 25km and confirmed the lateral inhomogeneity of the upper crust and the gradational velocity structure of the entire crust. More importantly, this study also concluded that the material with velocity up to Vp=7.5 km/s is gabbroic and not mantle peridotic.

About a decade ago, Du & Foulger [1999, 2001] and Du *et al.* [2002] applied the receiver function technique and produced a suite of crustal structures covering most of Iceland using data from the Iceland Hotspot Project. In addition to a naturally layered model, these studies also determined a low velocity zone in the lower crust and found a gradual velocity transition zone across the Moho. The thickest crust is found beneath the MVZ, NVZ, and EVZ from receiver functions [Foulger *et al.,* 2000, 2001].

In 2000, Darbyshire *et al.* built an Iceland crust model using seismic data and gravity data. Subsequently, they assembled all seismic reflection and receiver function results then available and used the gravity field to estimate the crustal thickness beneath regions that are not sampled seismically (Figure 5). They concluded that the thickness of Iceland crust varied from 40 km beneath northwestern Vatnajokull due to high mantle temperature and active upwelling in a narrow plume core to 15 km southwest due to a large distance from the mantle plume. They also pointed out that lateral density variation should be introduced into the mantle beneath rift zones to fit both seismic and gravity data.

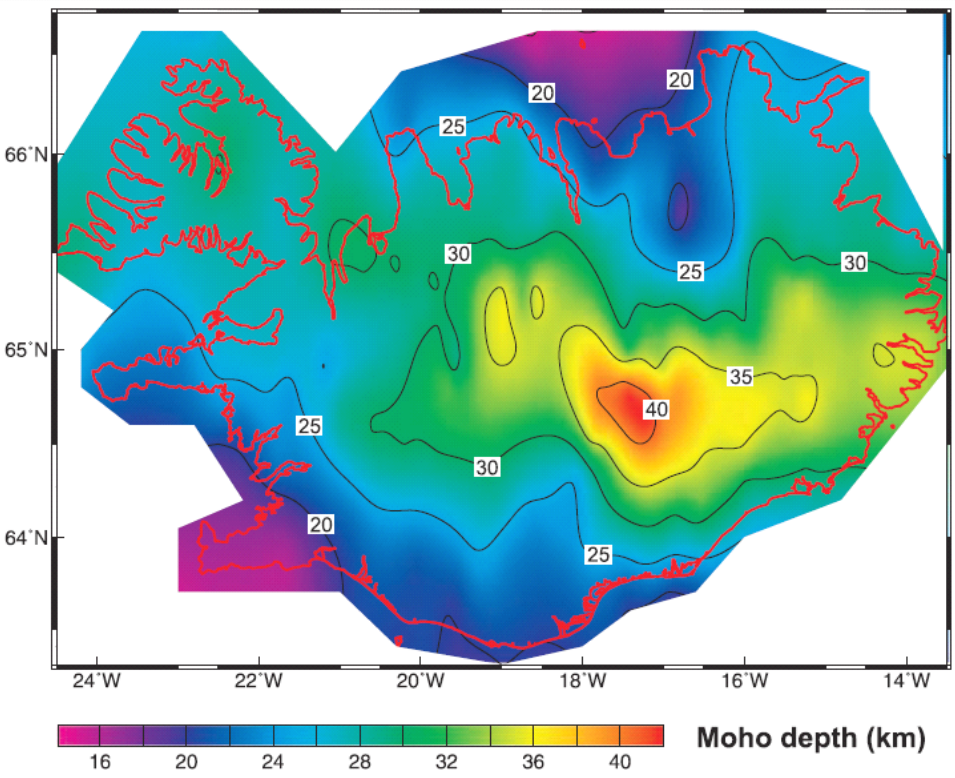

Figure 5 *Contour map of total crustal thickness determined using combination of seismic and gravity method. [Darbyshire et al., 2000]*

2.1.3 The thick-hot crustal model

In 2002, Allen *et al.* published a 3D shear wave model for Iceland crust using combination of body wave and surface wave constraints and proposed a thick-hot crustal model. 3D crustal S velocity and the Moho depth were acquired from this study. The model was obtained by fitting Love waves from six local events, Sn travel times from the same events, as well as the previous observations of crustal thickness. They observed a circular low velocity anomaly under the current hotspot in the lower crust and extended low velocity band along rift zones in upper crust. This observation

led to the interpretation of a thermal halo of a plume-driven plumbing system, where magma is fed from the core of the mantle plume vertically up through the lower crust in central Iceland and then laterally along the upper crustal rift system. This plumbing hypothesis suggests that the magma that passes through lower crust up to upper crustal chambers takes responsibility for the bulk of crustal formation [Allen *et al.*, 2002] (Figure 6).

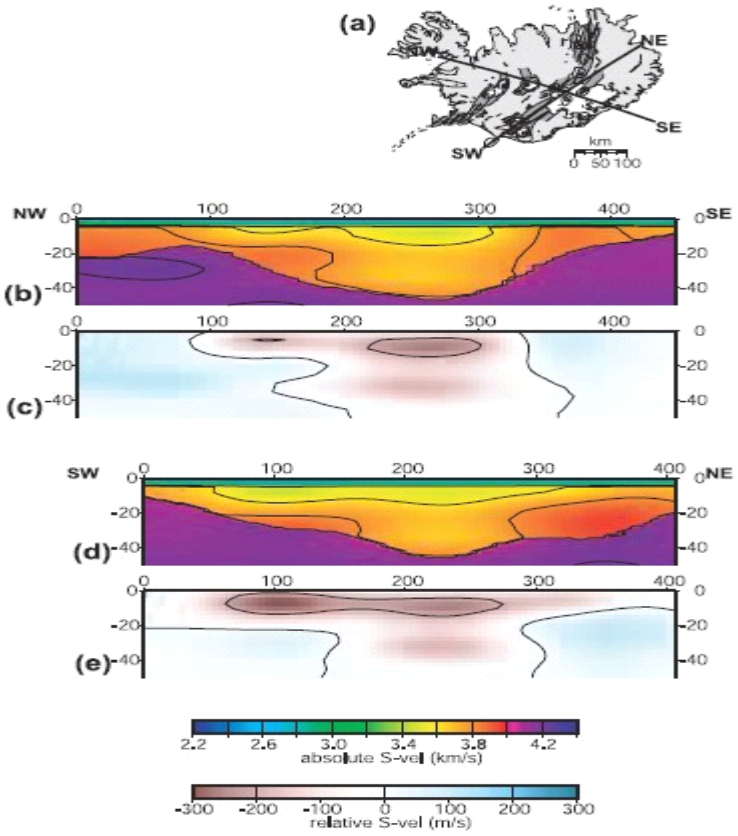

Figure 6 *Vertical slices through the velocity structure of Iceland, parallel and perpendicular to the Eastern Neovolcanic Zone. Purple colors correspond to mantle velocities. [Allen et al., 2002]*

2.2 Other famous crustal studies in Iceland

Basalt lava flows In Iceland erupted during the last 15 million years, which are the best available material for studying magnetic field variation in Iceland. Paleomagnetic research in Iceland has had two major objectives: to aid in local stratigraphic mapping and formation age estimation; and to obtain information on certain properties of the geomagnetic field, such as its reversals, other variations, and long-term average configuration.

High magnetic anomaly has been presented in central Iceland volcanic complexes. The rock, in other cases dike or sheeted swarms, is interpreted as gabbro. [Kristjansson *et al.,* 1998]. Another magnetic survey is focused on the Katla volcano [Jonsson and Kristjansson, 2007], which marked by 8km by 12km negatively anomaly of around 2000nT compared with the regional field (Figure 7). Jonsson and Kristjansson [2007] believed that this negative anomaly is mostly caused by the absence of remanent magnetization in the crustal rocks due to high temperature associated with magma chamber beneath the volcano and the destruction of magnetic materials in the upper crust. Due to the limited depth resolution in these magnetic data, the magnetic study provides little information about the lower crustal formation.

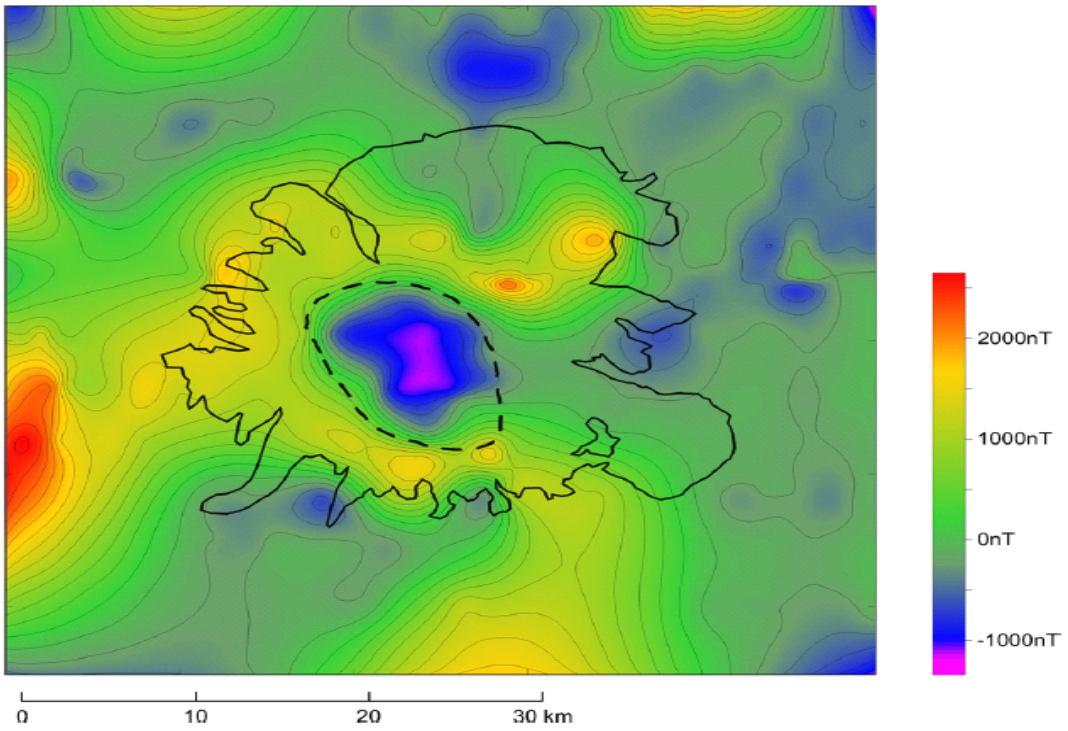

Figure 7 *Residual magnetic field over Katla volcano. [Jonsson and Kristjansson 2007]*

Li and Detrick [2003] have determined the pattern of azimuthal anisotropy in Iceland. They found that fast directions from shear-wave splitting are roughly N-S in western Iceland and NNW-SSE in the eastern Iceland. However, anisotropy form shear-wave splitting is largely attributed to mantle origin. They also solved azimuthal anisotropy from Rayleigh wave tomography and observed ridge-parallel fast direction at 25-40s and weak anisotropy at 50-67s and draw a conclusion that the buoyant flow associated with mantle plume is significantly channeled along the Mid-Atlantic Ridge (Figure 8) . However, the shortest period used by Li and Detrick [2003] is 20 s, which has poor sensitivity to upper and mid crust. In addition, radial anisotropy in Iceland that requires constraints from both Rayleigh and Love wave phase velocities has not

been developed in Iceland. Since previous studies have obtained Rayleigh wave phase velocities, the missing component is Love wave phase velocity maps, which is the main objective of this study.

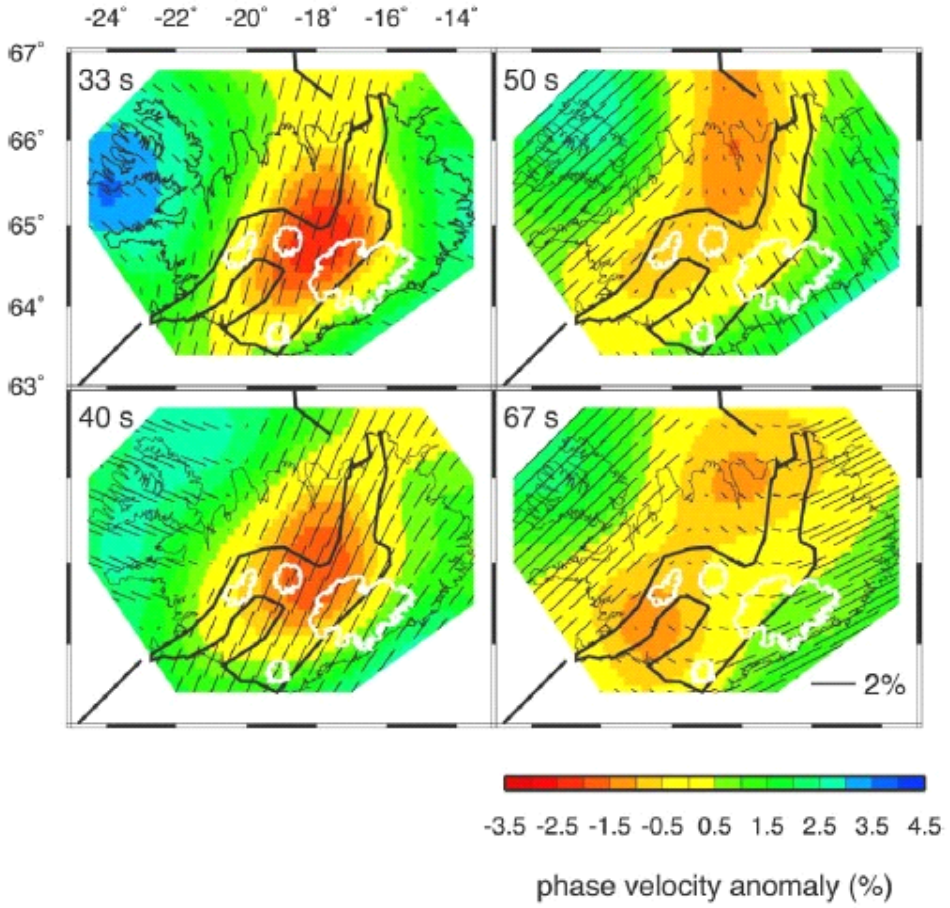

Figure 8 *Maps of phase velocity and azimuthal anisotropy at four periods (33, 40, 50, and 67 s). Color contours are isotropic phase velocity perturbations relative to the average values Black bars indicate anisotropy in a map view. Strike of bars represents orientation of fast directions and bar lengths are proportional to the magnitude of anisotropy. Thick black lines mark the Mid-Atlantic Ridge rift zones. White lines are for icecaps. [Aibing Li & Detrick, 2003]*

Gudmundsson *et al*. [2007] utilized a new technique, ambient seismic noise method, to study the Icelandic crust. They derived Rayleigh wave group velocities at three different frequencies by cross-correlating 2 years of ambient noise from 31 broadband stations distributed across Iceland (Figure 9). The group velocity maps show low velocity zone coinciding with rift zone and young crust in central Iceland while higher velocity is obtained in older volcanic areas.

Azvedo *et al*. [2012] conducted Rayleigh wave tomography using ambient seismic noise data recorded at the HOTSPOT experiment, which consisted of 30 broadband seismic stations and operated from June of 1996 to August of 1998. Phase velocity maps (Figure 24) at periods from 5s to 35 s were produced from the ambient noise tomography. These maps present low velocities at the active volcanic zones and mid-Atlantic ridge in Iceland. Shear-wave inversion and shear-wave velocity in the shallow crust maps shows a more spread-out distribution of low velocity anomalies along all active regions, which is probably associated with partial melt that feeds the local volcanoes. The lower crust map presents a more concentrated low velocity anomaly mainly beneath the Iceland hotspot, indicating melt accumulation and/or high temperature from the Iceland plume.

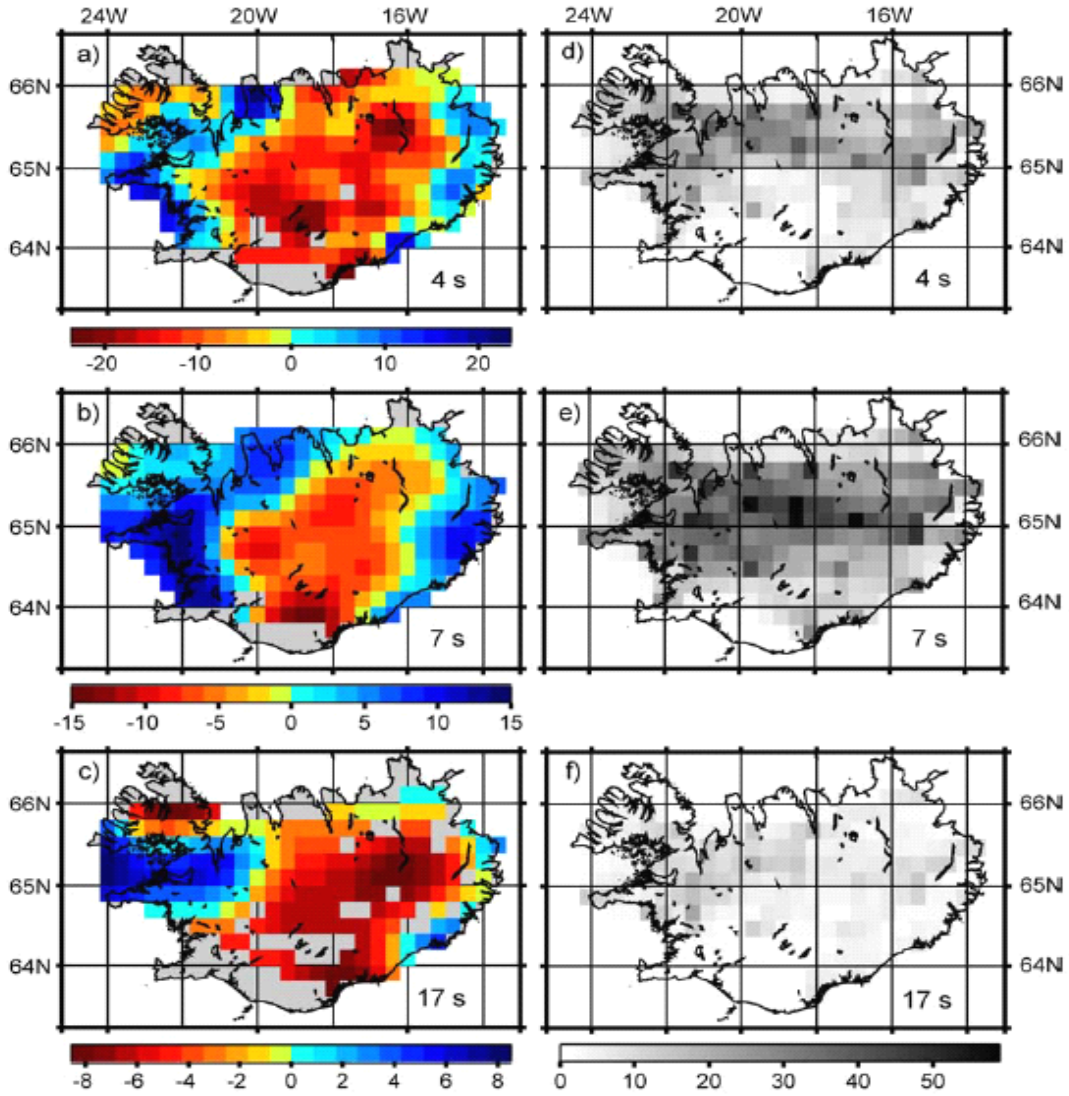

Figure 9 *Group velocity maps(left) and hit counts maps(right) for three different frequency bands used in ambient noise data process in Iceland. [Gudmundsson et al., 2007]*

Chapter 3 Data origin and data analysis

3.1 Data origin

The ambient noise data used in this study is recorded by the HOTSPOT experiment that consisted of 33 broadband instruments, with Reftek recorders. The instruments were installed between May 28 and July 31, 1996 and dismantled in July 1998 (Figure 10). The locations were chosen to be spaced evenly over the island while being near a connection to the power grid where possible [Allen *et al.*, 2002]. Several HOTSPOT stations failed during the experiment but data loss was minimized by regular station visits and checks. Seismic records from July 1996 to July 1998 were obtained from the IRIS Data Management Center via the standard data request tools.

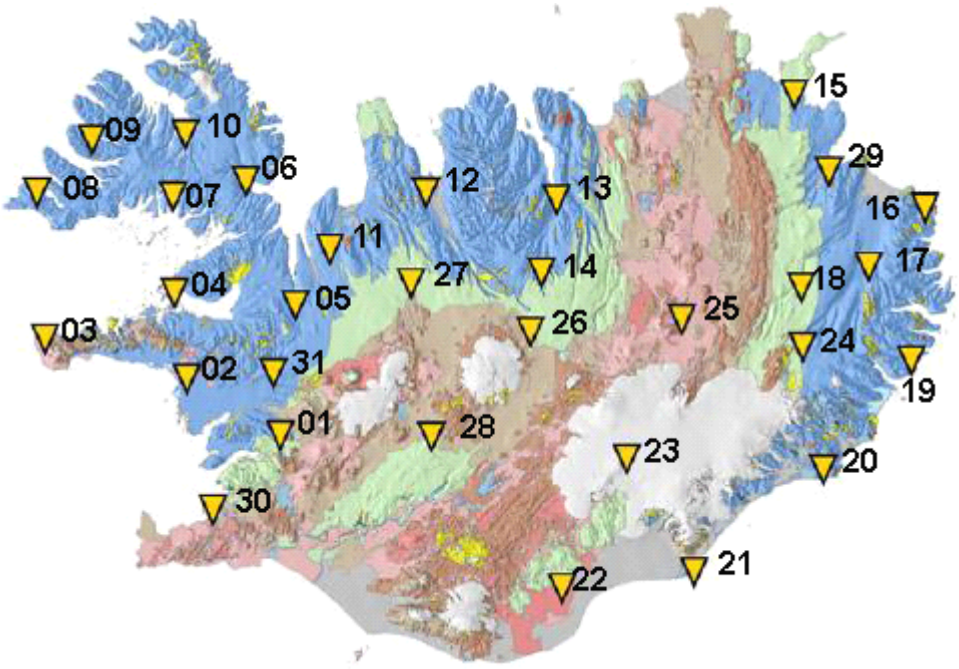

Figure 10 *Maps of the 31 HOTSPOT stations.*

3.2 Ambient noise data analysis

Ambient seismic noise is generated mainly by nearby human activities (such as traffic, heavy machinery), winds and other atmospheric phenomenon, and ocean waves. It was once considered to be useless in the past and always causes troublesome in data processing. Numerous methods have been developed to reduce its negative effects. However, recent results from other research domain have revealed that ambient noise, in fact, contains lots of useful information for studying earth structure.

Theoretical and experimental researches have shown that an estimate of the Green's function between two points can be obtained from the cross-correlation of ambient noise recorded at the two locations [Weaver & Lobkis 2001, 2004; Lobkis & Weaver 2001; Derode *et al.,* 2003; Snieder 2004; Wapenaar 2004; Larose *et al.,* 2005; Roux *et al.,* 2005a]. Shapiro and Campillo. [2004] first applied this method to seismology. They computed cross-correlations of vertical component between different stations and successfully extracted Rayleigh wave empirical Green's Function whose dispersive characteristics are similar to those predicted from earthquake. This provides a new source of surface wave measurement without earthquake occurrence. From that time on, ambient noise tomography based on empirical Green's Function extracted from cross-correlation has been widely used all around the world. First real ambient noise tomography was applied between stations in California and produced meaningful results correlated with geological units

[Shapiro *et al., 2005*]. Then this method was applied in Tibet [Yao *et al*., 2006], South Korea [Cho *et al*., 2006], Europe [Yang *et al.,* 2007], New Zealand [Lin *et al*., 2007], and Iberian Peninsula [Villaseñor *et al*., 2007]. But these studies only focused on short periods as Shapiro did. Broadband applications, which can expand study depth, were applied to large areas such as Europe [Bensen *et al*., 2005]. In addition, the procedure to use long-duration cross-correlations to study the long-range correlation properties of ambient seismic noise was developed by *Stehly et al*.[2006]. This improvement increased signal-noise ratio significantly.

In 2007, Bensen *et al*. made great progress and offered a detailed approach to processing seismic ambient noise data to gain reliable broad-band Rayleigh wave measurement (Figure 11). The advantages of using seismic ambient noise are summarized as follows.

(1) The measurements from seismic noise depend on station configuration rather than earthquake location that is often in limited directions.

(2) Unlike conventional seismic methods source location and intensity are not of principal concern in seismic noise measurements.

(3) The resolution from seismic noise data can be improved by increasing the number of stations and reducing the station spacing.

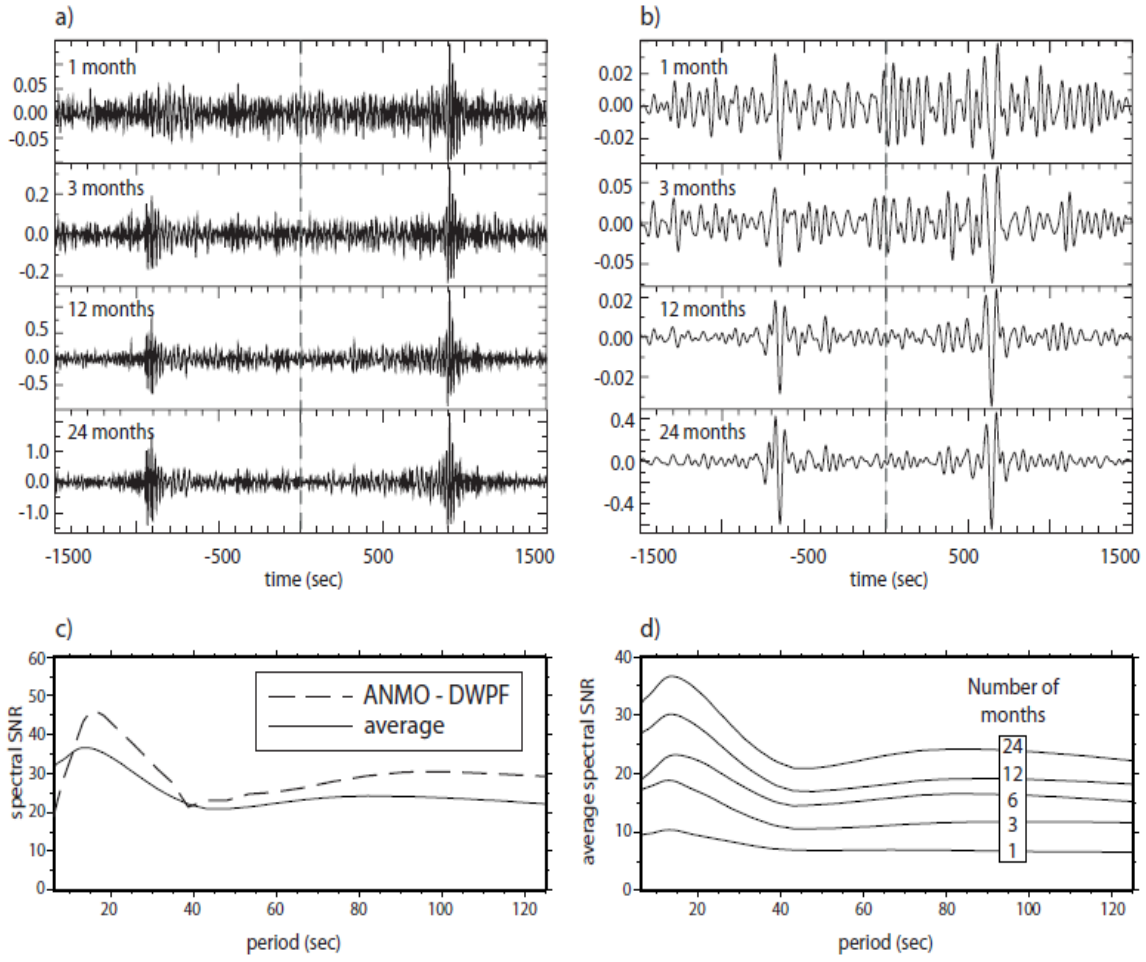

Figure 11 *Example of the emergence of the Rayleigh waves for increasingly long time-series. [a] Cross-correlations at the specified time-series lengths for the station pair ANMO and DWPF [DisneyWilderness Preserve, FL, USA] band passed between 5 and 40 s period. [b] Same as [a], but for a passband between 40 and 100 s period. [c] Spectral SNR for the 24-month ANMO-DWPF cross-correlation shown with a dashed line, and the spectral SNR averaged over all cross-correlations between GSN stations in the US shown with a solid line. [d] Spectral SNR averaged over all cross-correlations between GSN stations in the US for different time-series lengths of 1, 3, 6, 12 and 24 months. [Bensen et al., 2007]*

(4) It can be used to measure phase velocities at short periods (< 40 s) that are usually hard to determine using earthquake data and therefore help to provide better constraint on crustal structure.

Although Love waves, the other kind of surface wave, can also be extracted from cross-correlation of horizontal component between diffuse wave field, early studies only focused on Rayleigh wave because people believed that ambient seismic noise source would be ineffective at directly generating Love waves. Lin *et al.* [2008] described a method for extracting Love wave phase velocities from ambient noise cross-correlation and applied it to the western US.

Following Lin *et al.* [2008], I processed horizontal ambient noise data at the HOTSPOPT stations to obtain Love wave phase velocities. The procedures for data analysis can be divided into single station data processing and cross-correlation and stacking.

3.2.1 Single station processing

I acquired north component and east component (N, E) broad-band ambient seismic noise data at 33 HOTSPOT stations in Iceland from July, 1996 to July, 1998. All data were processed on a daily basis and then were stacked later. Figure 12 shows an example waveform of ambient noise that contains a broadband scattered waves propagating in all possible directions. All original ambient seismic data were modified to one sample per second to reduce the size of data. Then mean and trend were

removed for noise data at each station. All daily records were cut to the same window length (3000s-80000s) to assist processing in next steps. Because the instrumental irregularities tend to obscure signal of ambient noise, I removed instrument response from the data as well. Data were further processed to minimize the effects of large amplitude signals in both the time and frequency domain. Temporal normalization was applied to reduce the effect of earthquakes, instrument irregularities, and nearby non-stationary noise sources on the ambient noise cross-correlations [Bensen *et al.,* 2007].

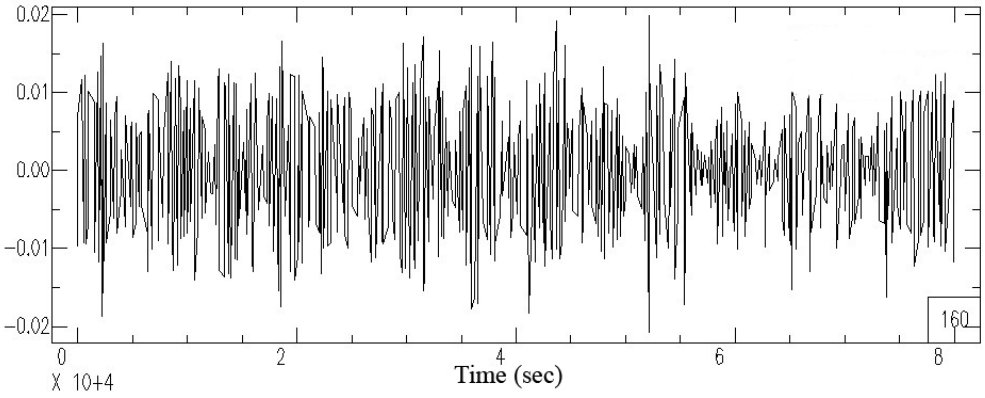

Figure 12 *Example of raw ambient noise data used in this study.(March 1,1997 station 12, N component)*

Because the raw data in this study are only north and east components of ambient noise, in order to retrieve Love wave that polarizes perpendicular to the ray path as an SH wave, N E components have to be rotated to radial (R) and transverse(T) direction for each station pairs. North-north, south-south, north-south, and south-north components of ambient noise between each station pairs for one day length can

be obtained from the pre-processed data. Because the latitude and longitude of each station in HOTSPOT array are known, the interstation azimuth θ and backazimuth ψ angles can be calculated. Finally, with these angles, transverse–transverse, transverse–radial, radial–radial, and radial–transverse component of ambient noise can be calculated by applying the rotation operator in equation 1. Note that both the radial components and the transverse components at a pair of stations point to the same direction, respectively, (Figure 13).

$$\begin{pmatrix} TT \\ RR \\ TR \\ RT \end{pmatrix} = \begin{pmatrix} -\cos\theta\cos\psi & \cos\theta\sin\psi & -\sin\theta\sin\psi & \sin\theta\cos\psi \\ -\sin\theta\sin\psi & -\sin\theta\cos\psi & -\cos\theta\cos\psi & -\cos\theta\sin\psi \\ -\cos\theta\sin\psi & -\cos\theta\cos\psi & \sin\theta\cos\psi & \sin\theta\sin\psi \\ -\sin\theta\cos\psi & \sin\theta\sin\psi & \cos\theta\sin\psi & -\cos\theta\cos\psi \end{pmatrix} \times \begin{pmatrix} EE \\ EN \\ NN \\ NE \end{pmatrix}. \quad (1)$$

Equation 1 *Rotation operator used in this study to do rotation.*

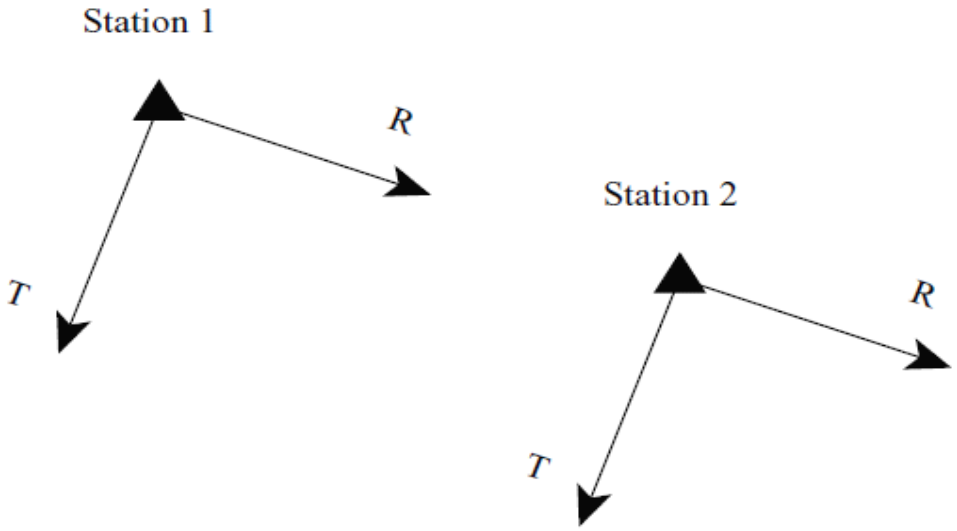

Figure 13 *Map shows the definition of radial and transverse components between two stations. [Lin et al., 2008]*

Additionally, data are whitened in frequency domain that aims to provide more comparable amplitude at all frequencies. It is clear that the amplitude of ambient noise is not flat in frequency domain after applying Fourier transform to the noise data. Obviously, a peak microseism is shown around period 7s and the amplitude rises again at very long periods above 40s (Figure 14 (a)). The exact generation mechanism of the microseisms is not clear, but it is commonly believed that the microseism contains direct interaction of ocean swells with the shallow seafloor [Hasselmann, 1963]. Inversely weighting the complex spectrum by a smoothed version of the amplitude spectrum produces the normalized or whitened spectrum shown in Figure 14 (b) [Bensen *et al.,* 2007]. Frequency whitening is carried out to broaden the frequency band of the dispersion measurement.

3.2.2 Cross-correlation and stacking

After finishing single station data processing, I cross-correlated transverse components of ambient seismic noise in frequency domain on a daily basis. Then the result of cross-correlation of same station pairs were inverted to time domain and added to each other. According to Bensen *et al.* [2007], stacking of 1-year data can produce reliable Green's functions. Consequently, data were stacked every month and then every year. In this study, the stacking results were not very reliable in June, 1996. So the data of this month were not used in the final stacking. The resulting Love wave signals emerged at both positive and negative correlation lags as shown in Figure 15. The positive single is usually called 'causal' and the negative one is called 'acausal'.

If the distribution of ambient noise is uniform, the positive and negative signals should be identical and symmetrical. However, asymmetrical negative and positive seismograms are very commonly observed, indicating unevenly distributed noise sources. Two profiles (HOT01-HOT11 and HOT09-HOT12) were selected and shown in Figure 16. The correlation for HOT01-HOT11 is highly asymmetrical, where the positive correlation signal is much stronger than the negative one.

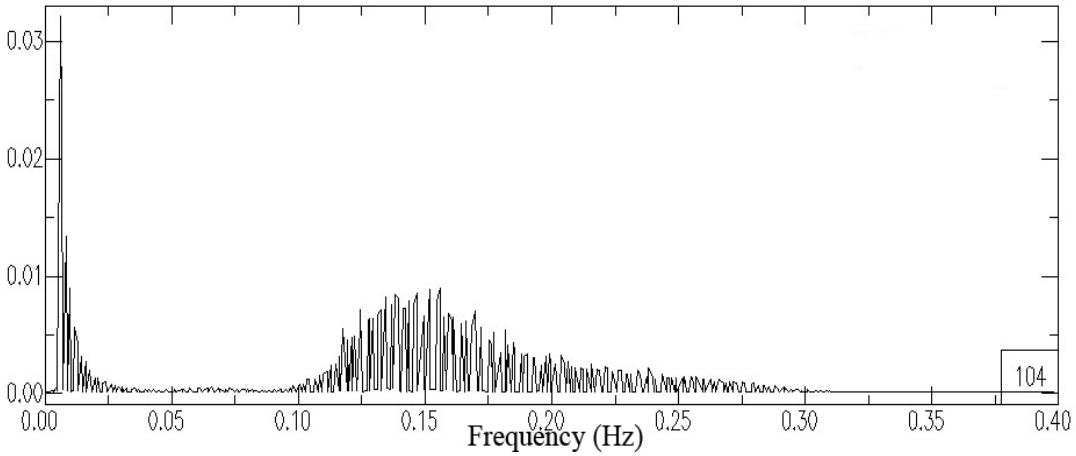

(a)

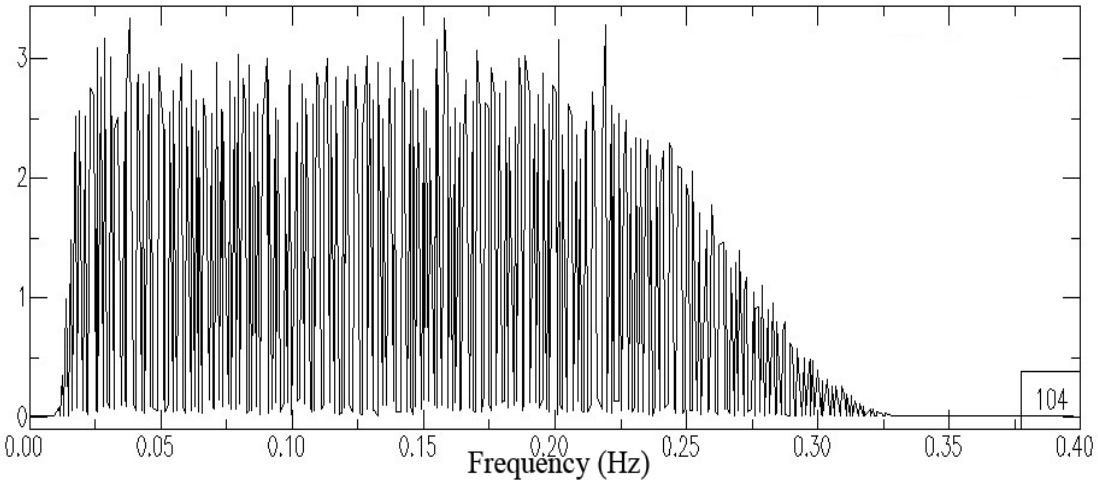

(b)

Figure 14 *(a) represents raw amplitude spectra for one sample per second radial component at station HOT10 on March 8, 1997. (b) represents spectrally whitened raw data.*

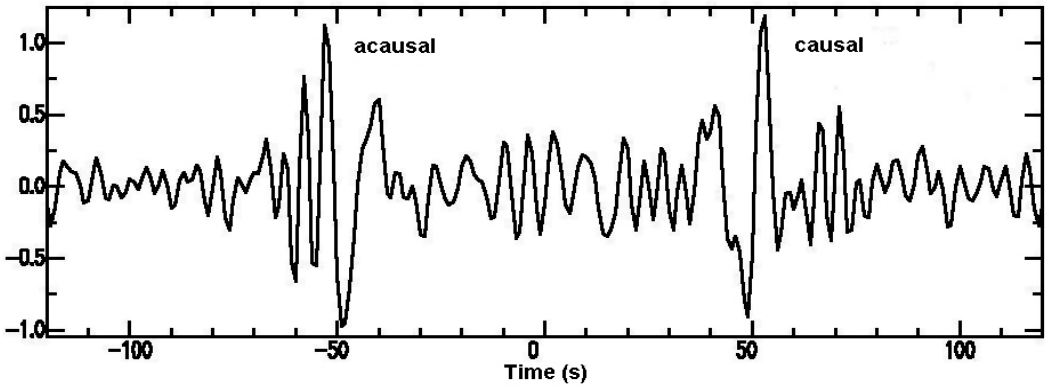

(a)

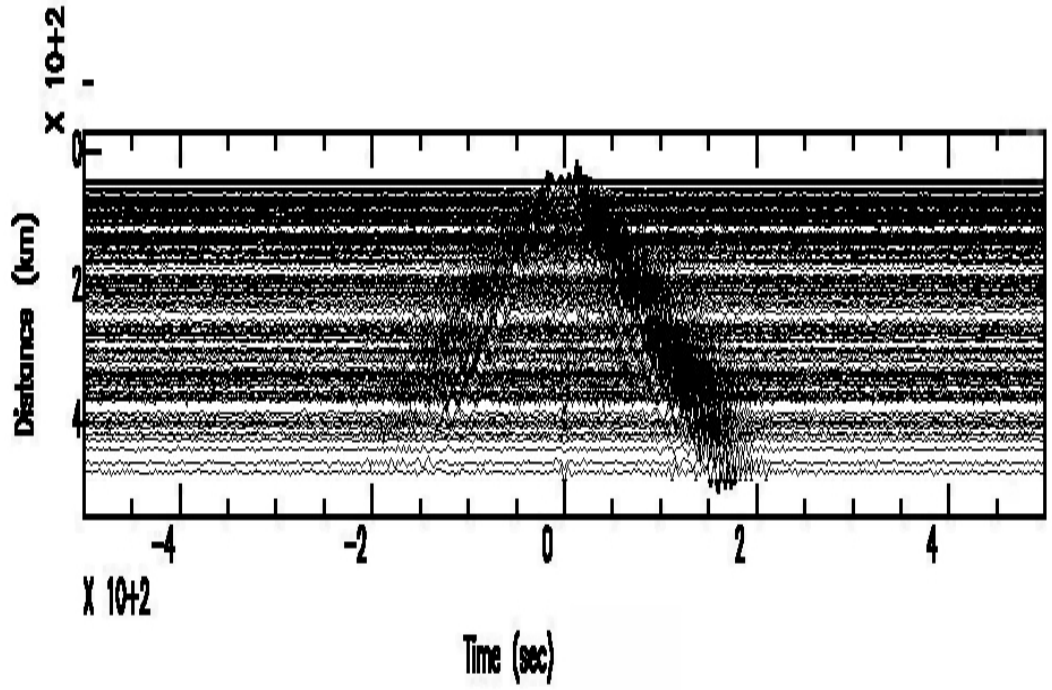

(b)

Figure 15 *(a) Cross-correlated and stacked ambient seismic noise data for a station pair HOT08-HOT11. (b) represents cross-correlated and stacked transverse-transverse components Ambient Seismic Noise data from Iceland processed from all two years of the HOTSPOT experiment. These waveforms have been sorted by distance between station pairs and show the fundamental mode Love waves.*

The positive and negative lags here represent different propagation directions of the Love wave, meaning from station HOT01 to HOT11 or from HOT11 to HOT 01, respectively. This type of robust, asymmetric correlation peaks exhibited by profile 1 favor a single, dominant noise. Because positive correlation signal is stronger than the negative one, indicating the dominate source is located to the south of HOT01, and might be along the Reykjanes ridge. These asymmetric correlations are also observed in other paths along NS direction, suggesting the intensity of ocean waves is strong from south. The correlated seismogram between station HOT09 and HOT12 that are aligned in roughly EW direction presents a symmetric correlation stack. In this case the direction of dominant ambient noise from south is perpendicular to the ray path and therefore does not generate asymmetry in the correlated signals. Although accurate location of the dominant noise source is interesting, it would require further modeling and is beyond of the main scope of this study.

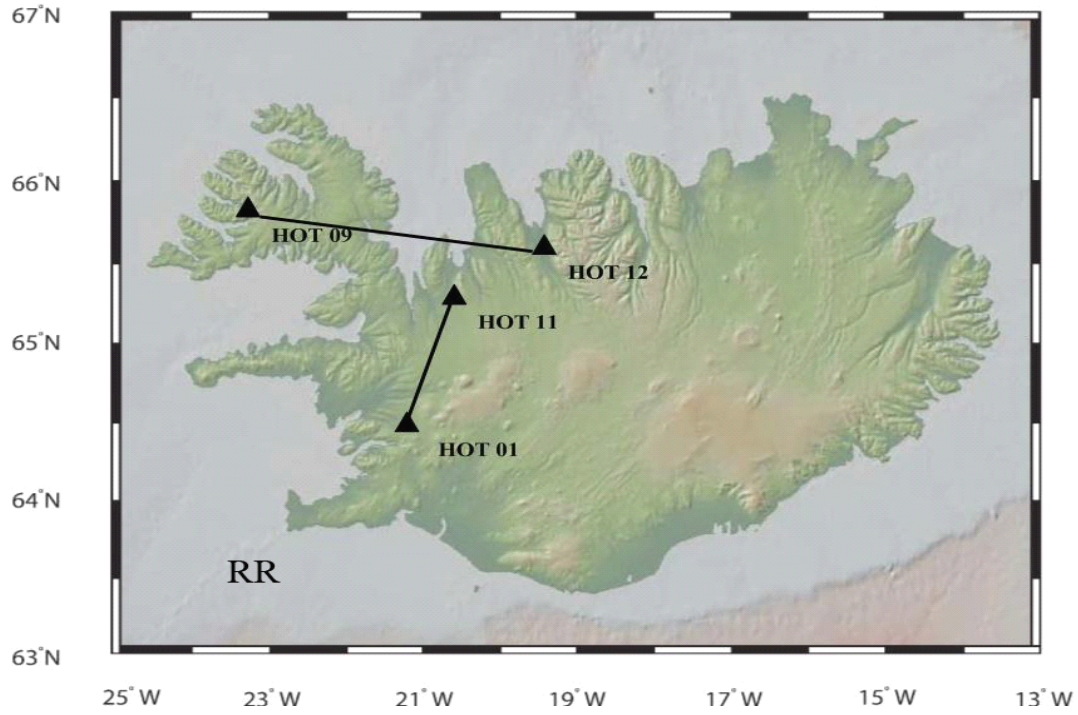
67°N
66°N
65°N
64°N
63°N
25° W
23° W
21° W
19° W
17° W
15° W
13° W
HOT 09
HOT 12
HOT 11
HOT 01
RR

(a)

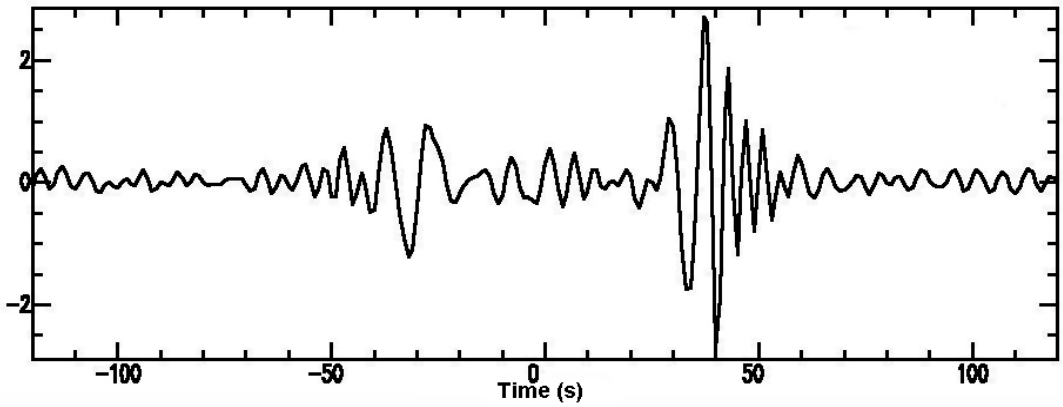
2
0
-2
-100
-50
0
50
100
Time (s)

(b)

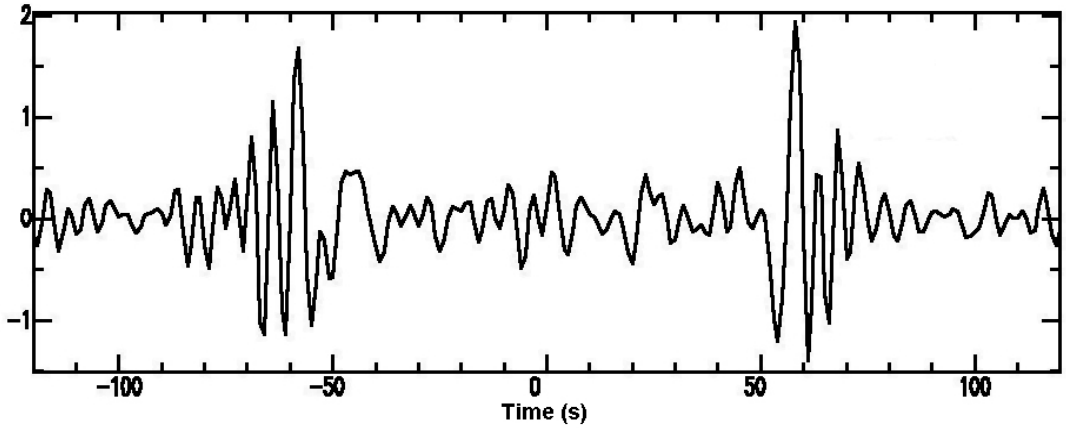

(c)

Figure 16 *(a) shows the location of profile 1 and profile 2. RR here represents Reykjanes ridge. (b) is the waveform emerged after cross correlation between HOT 01 and HOT 11. It is quite obvious that positive and negative components are asymmetric (c) reflects the situation between HOT 09 and HOT12. Here the waveform of two components are almost the same.*

In order to increase signal-to-noise ratio and reduce the effect of asymmetry in the cross-correlation, each cross-correlated waveform was divided into positive and negative components and were added together to create a final symmetric cross-correlation as shown Figure 17. The subsequent data processing phases are applied only on these symmetric cross-correlated waveforms.

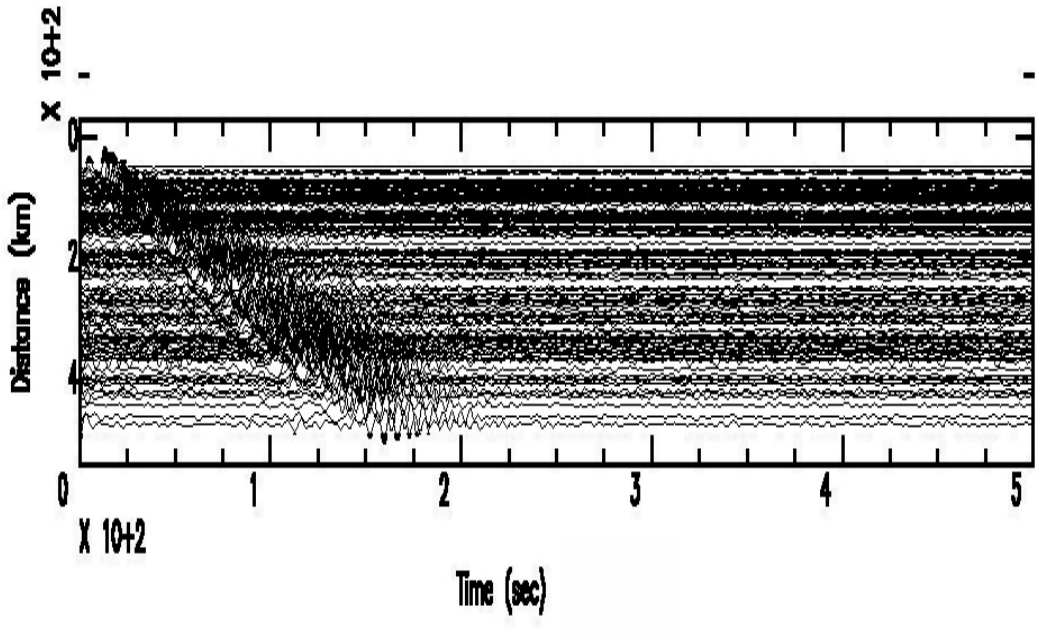

Figure 17 *Symmetric-component cross-correlation and stacked transverse-transverse components of Ambient Seismic Noise data from Iceland processed from all two years of the HOTSPOT experiment. These waveforms have been sorted by distance between station pairs.*

In order to quantify the strength of Love wave signals, the signal and noise window are defined and average signal noise ratios (SNR) of different periods are calculated as shown in Figure 18. For each station pair we calculate the spectral SNR by computing the ratio of the signal peak in the predicted arrival window to the root mean square (rms) of the noise trailing the arrival window, in each period band for the symmetric component cross-correlation. Love wave SNR shows a single peak at periods 14 s and drop rapidly above 20s. This drop may result from increasing effect

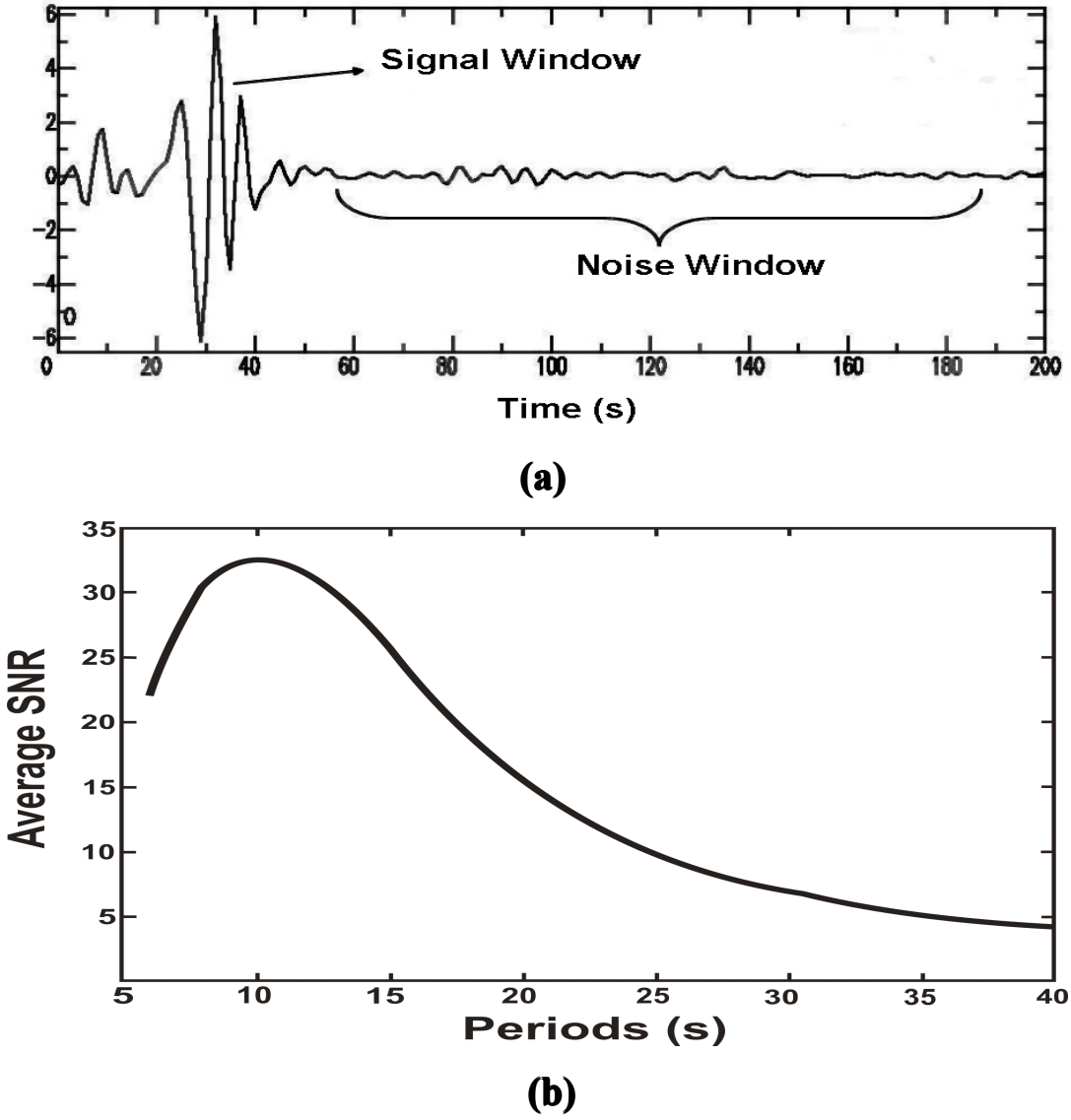

Figure 18 *(a) Waveform with defined noise window and signal window.(b) Average Single-to-Noise ratio for Love wave. Only the distance of station pair larger than three wavelengths contributes to this average SNR.*

of noise contamination and decay of signal. In addition, unfortunately, the Love wave signals are not obvious and SNR is relatively low in July, 1996, which has bad a effect on the final stacking result. As a consequence the data from the months of July of 1996 were removed and the utilized data ranged from August 1996 to July1998.

Chapter 4 Love wave phase velocity

4.1 Phase velocity calculation

Theoretical studies by Lobkis & Weaver [2001], Roux *et al.* [2005], Sabra *et al.*[2005b] and Snieder [2004] have shown how to extract estimated Green's function under the assumption of homogeneous source distribution. The relationship between cross-correlation of station A and station B (C(t)) and estimated Green's function(G(t)) are shown here.

$$\frac{dC_{AB}(t)}{dt} = -G_{AB}(t) + G_{BA}(-t)$$

If the source of ambient noise is randomly distributed, the positive part and the negative part of cross-correlation should be symmetric. This is not true at many times due to the unevenly distribution of microseismic noise.

To optimize signal bandwidth, enhance SNR, and simplify the calculation, the positive and negative signals are averaged to form a single trace. The final estimated Green's function can be expressed as

$$G_{AB}(t) = -\frac{d}{dt}\left[\frac{C_{AB}(t) + C_{AB}(-t)}{2}\right]$$
$$0 \le t < \infty$$

Green's functions are produced from the averaged cross-correlations are used to calculate phase velocity from an automatic frequency-time analysis. Waveform f(t)

can be transferred to complex function A(t)exp[iφ(t)], where A(t) represents envelop and φ(t) is phase function. The group travel time, marked by t, can be directly measured from a seismogram. Then the group velocity can be easily calculated if the distance of the two stations represented by r is known from simple equation r/t. Although many ambient noise studies before only focused on measuring the group velocity of surface waves, we decided to measure phase velocity instead due to certain factors. First the uncertainty of phase velocity measurements is smaller than that of group velocity. Secondly phase velocity has a greater sensitivity for deeper structures. Third, group velocity can be calculated from the dispersion of phase velocities but the opposite cannot be done.[Bensen *et al.*, 2007].

The corresponding instantaneous frequency can be determined by w=[∂φ(t)/∂t]. The phase component can be expressed below:

$$\varphi(t) = kr - \omega t + \frac{\pi}{2} - \frac{\pi}{4} + N.2\pi + \lambda$$
$$N \in Interger \quad , \lambda \in \mathrm{Re}$$

where k is the wavenumber, $\pi/2$ is the phase shift from the negative time-derivative, $-\pi/4$ is the phase shift due to the interference of a homogeneous source distribution $N \cdot 2\pi$ is the intrinsic phase ambiguity of phase measurement, and λ is the source phase ambiguity term or 'initial phase' that arises from the uncertainty of the source distribution in addition to other factors [Lin *et al.*, 2007]. From the definition of phase

velocity and equation above, phase velocity of the estimated Green function can be expressed as

$$c = \frac{\omega}{k} = \frac{r\omega}{[\varphi(t_{\max}) + \omega t_{\max} - \frac{\pi}{4} - N.2\pi - \lambda]}$$

N and λ are still unknown, however, N can be determined from two steps method and λ can be found from three stations methods [Lin *et al.*, 2008].

4.2 Phase velocity dispersion curves

Love wave phase velocity in Iceland is calculated at 12 periods from 6 to 40 s (6s, 8s, 10s, 12s, 14s, 16s, 18s, 20s, 25s, 30s, 35s, 40s). Love wave phase velocity combined with Rayleigh wave phase velocity derived by Azevedo *et al.* [2012] between three station pairs are selected to show phase velocity change in different areas of Iceland (Figure 19). The three station pairs are HOT23-HOT32 in western Iceland (blue line), HOT34-HOT32 in eastern Iceland (green line), and HOT21-HOT32 in central Iceland (red line). For each station pair the velocity of Love wave is higher than velocity of Rayleigh wave and absolute phase velocities all increase with period. Furthermore, it is quite obvious that phase velocity in central and southern Iceland is much slower than that in eastern and western Iceland. The low phase velocity in central and southern Iceland can be interpreted as the existence of

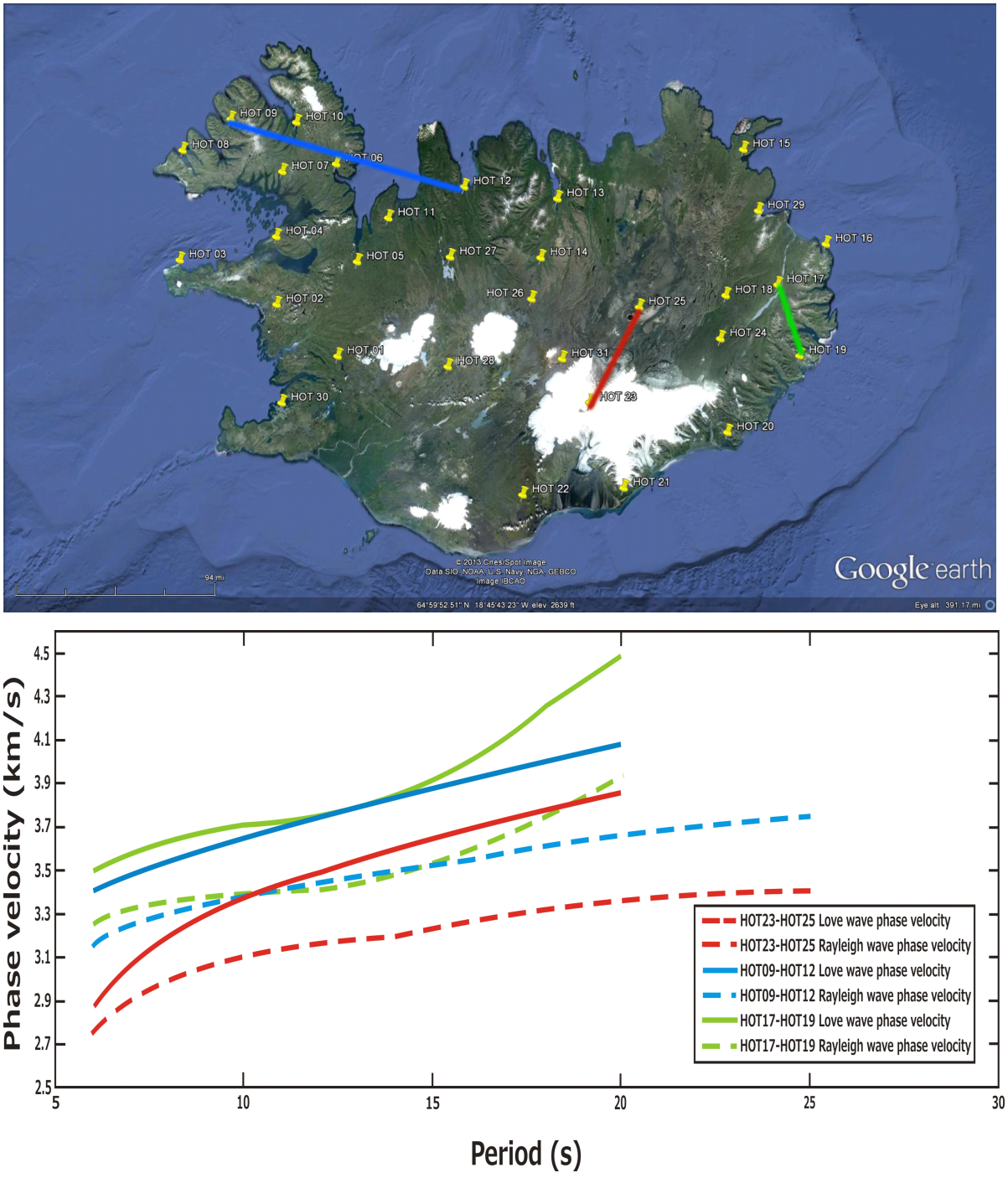

Figure 19 *Comparison of absolute phase velocities from different pairs of station. The pairs of stations number 23 to 25 is located in more seismically active areas and show lower phase velocity values than stations pairs 9 to 12 and 17 to 19, which are located in northwestern and eastern Iceland.*

high temperature and partial melt due to the hotspot and ridges. In eastern and western Iceland, the phase velocity is higher because these areas are far from current rift zones and the crust in these regions has been cooled down.

Average phase velocity in Iceland was calculated as well. Figure 20 shows the average dispersion curves of Love wave (this study) and Rayleigh wave [Azevedo *et al*., 2012). The average phase velocity varies from 3.13 km/s at period of 6s to 3.71km/s at 35s for Rayleigh wave and from 3.44 km/s at 6s to 3.96 km/s at 30s for Love wave. They are used as reference values for calculating phase velocity perturbations.

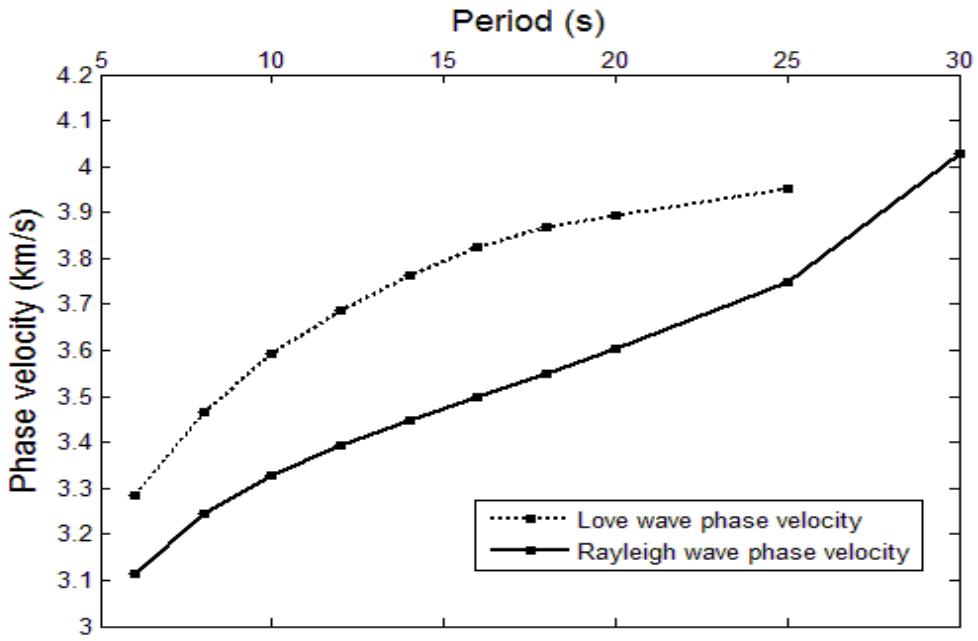

Figure 20 *Average Love wave and Rayleigh wave phase velocity measurement versus periods.*

4.3 Phase velocity maps

Phase velocity tomography is applied to Iceland after the average phase velocities for all available station pairs are determined. Following the method of Bensen *et al.* [2007], I parameterize the study region with grid interval of 0.5 degree. This method is based on minimizing a penalty function composed of a linear combination of data misfit, model smoothness and the perturbation to a reference model for isotropic wave speed [Yang *et al.*, 2007]. There are two important criteria for selecting phase velocity data. First, the distance between a station pair should be longer than three times of the wavelength to satisfy far-field approximation. Secondly, the SNR should be larger than 17 to be considered for Love wave tomography. Figure 21 shows the number of measurements that satisfy the two criteria mentioned above versus periods of Love wave. It is not surprise that this figure is similar to the SNR variation (Figure 18(b)) because the higher the SNR is and the larger number of high-quality measurements. The longest period for Love wave tomography is 25s due to the small number of measurements above 25s.

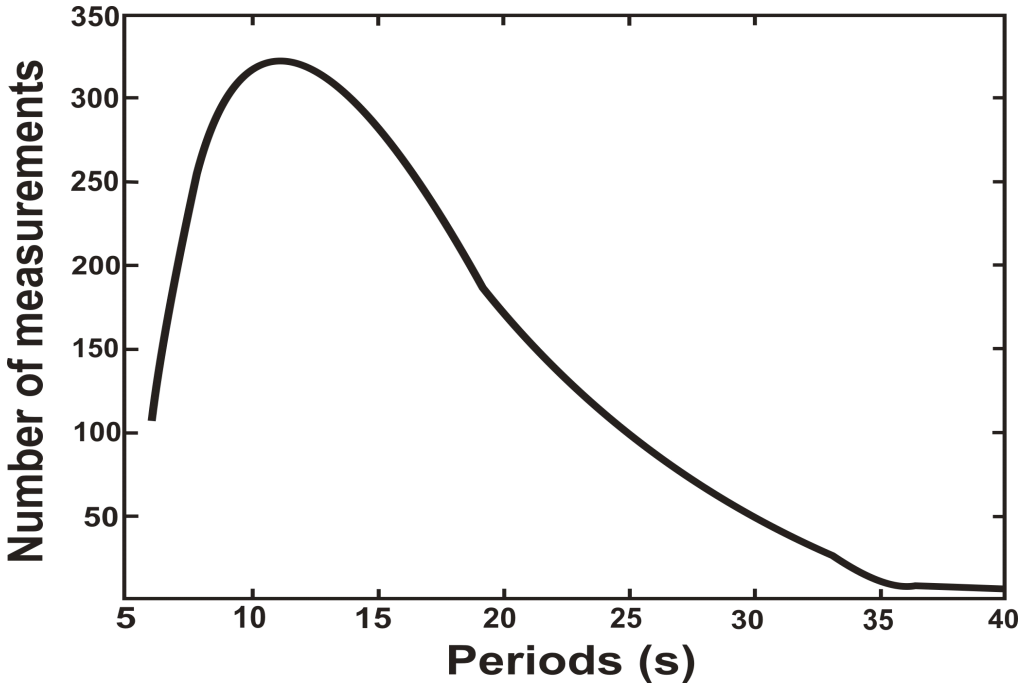

Figure 21 *Number of measurements which agree criterion with different periods.*

Figure 22 demonstrates the ray path coverage for Love wave tomography at different periods. It is clear that the number of high-quality data at shorter periods is much higher than at long periods. This systematic reduction in ray path density with period is largely due to the 3-wavelength constraint on distance. Given the location of the Hotspot array, it is obvious that the density of ray paths is the highest in central Iceland, resulting in high model resolution in this area. However, the number of ray path in southwestern and northeastern Iceland is small, especially for long periods, indicating poor model resolution in the tomography results in these areas.

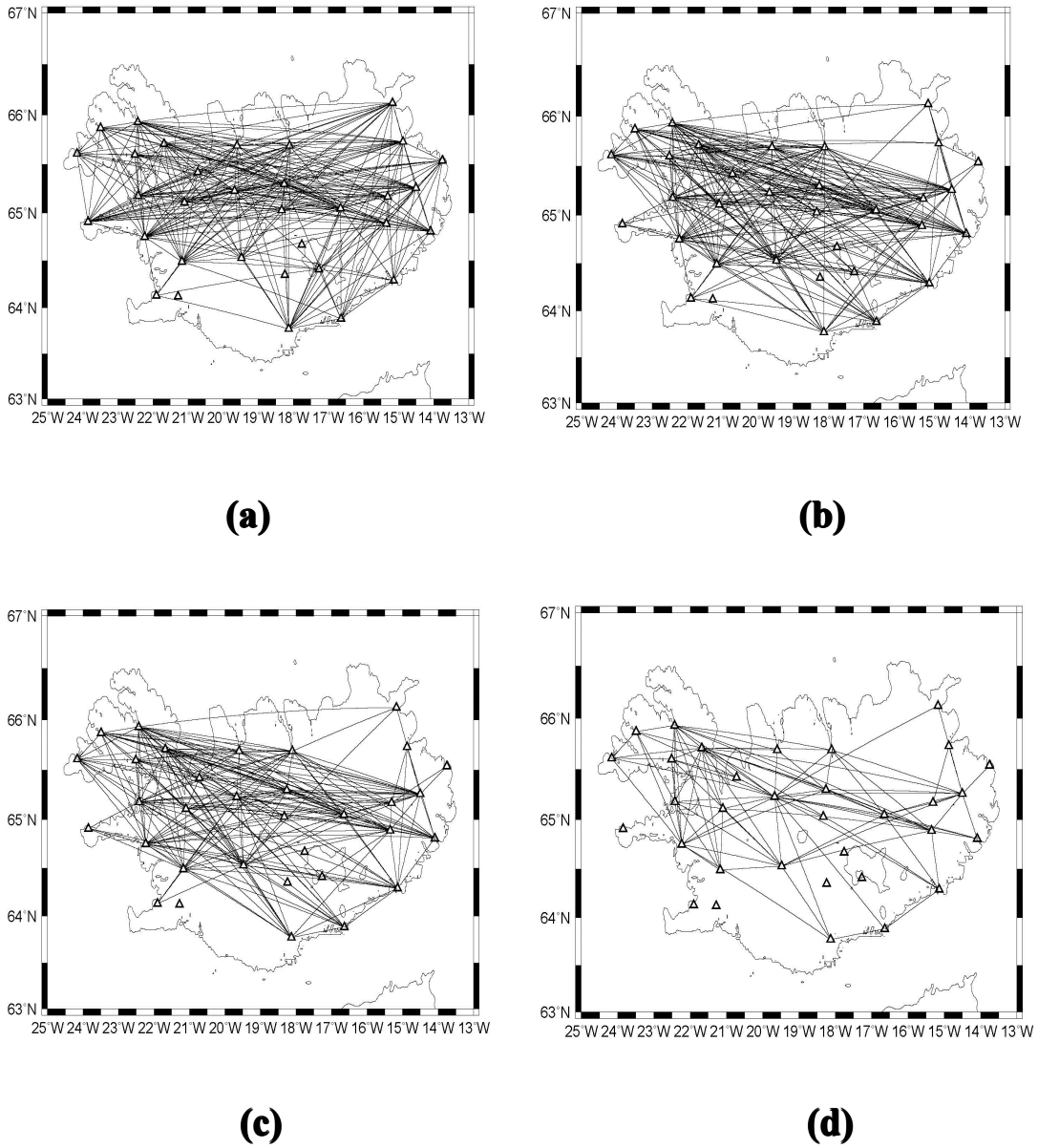

Figure 22 *Ray Path distribution of the station pair correlation phase velocity data at different periods of: 8 12, 16 and 20 seconds ((a), (b), (c), (d)) after the quality control filter of SNR > 17.*

Surface waves are dispersive and provide seismic constraints on crust and upper mantle structure. It is known that longer periods of surface wave can penetrate

to greater depths. In general, the peak sensitivity of Rayleigh wave is at the depth of 1/3 of the wavelength, while Love wave at the same period tends to be more sensitive to shallower depths. For instance in Iceland, shorter periods of Love wave, such as 8s, 10s, and 12s, can strongly reflect the structure of the upper crust while longer periods, such as 18s, 20s, and 25s, are more sensitive to the structure of the lower crust and uppermost mantle.

Figure 23 shows the Love wave phase velocity anomalies in the whole Iceland at different periods. Love wave at a period of 6s is most sensitive to the upper 10km of the crust. A large area of slow anomaly is the most profound feature of this figure. This low velocity anomaly extends along the MVZ, WVZ, and most part of EVZ and NVE. The largest anomaly, up to -6%, is found in the MVZ, at the location of the Hofsjokull glacier and Langjokull glacier. The highest phase velocity anomaly, up to 6%, is concentrated in northwestern Iceland, covering most of the Westernfjords region. The 8s, 10s, and 12s Love wave maps are sensitive to slightly deeper part of the crust compared with 6s Love wave map. The results of these maps are similar. Although low phase velocity is also found in central Iceland, it tends to be separated into two parts, one beneath Hofsjokull glacier, the other one beneath the volcanoes Bardarbunga and Grimsvotn, where the current hotspot is located. Variations of Love wave phase velocity at 14s, 16s, 18s, and 20s consistently exhibit similar features. The low velocity region gradually shrinks and concentrates on the MVZ and the location of the hotspot.

Rayleigh wave phase velocity in the same period range in Iceland was constructed by Azevedo *et al.* [2012] (Figure 24). The similarities of two studies are described below.

(1) Low velocity anomalies are largely found in central Iceland covering the MVZ, WVZ, and most part of EVZ and NVZ.

(2) Low velocity anomalies become less strong and more concentrated on the location of hotspot with the increasing of periods.

(3) Areas away from the mid-Atlantic ridges and the mantle plume are characterized by high velocity anomaly.

The phase velocity maps generally agree with the study of Gudmusson *et al.* [2007], who provided group velocity anomaly maps from Ambient Seismic Noise using the same data. Their study also showed slowest anomalies around central Iceland. These low velocity features can be interpreted as partial melt and high temperature caused by ridges and mantle plume in Iceland.

Although there are remarkable similarities between phase velocities results from this study and from the study of Azevedo *et al.*[2012], substantial differences are also present. For example, there is an obvious low velocity zone along the northern volcanic zone at periods 6s, 8s, 10s, 12s for Love wave, whereas Rayleigh wave phase velocity anomaly maps show this kind of low velocity anomaly at periods of 20s, 25s,

and 30s. Also, the strong low velocity anomaly is concentrated around Grimsvotn volcano and the Vatnajokull icecap at 8s for Love wave while this feature happens at longer period such as 14s and 20s for Rayleigh wave. These differences could reflect different structure at different depth and suggest the existence of anisotropy. A 3D model with anisotropy could better image the structure than phase velocity maps.

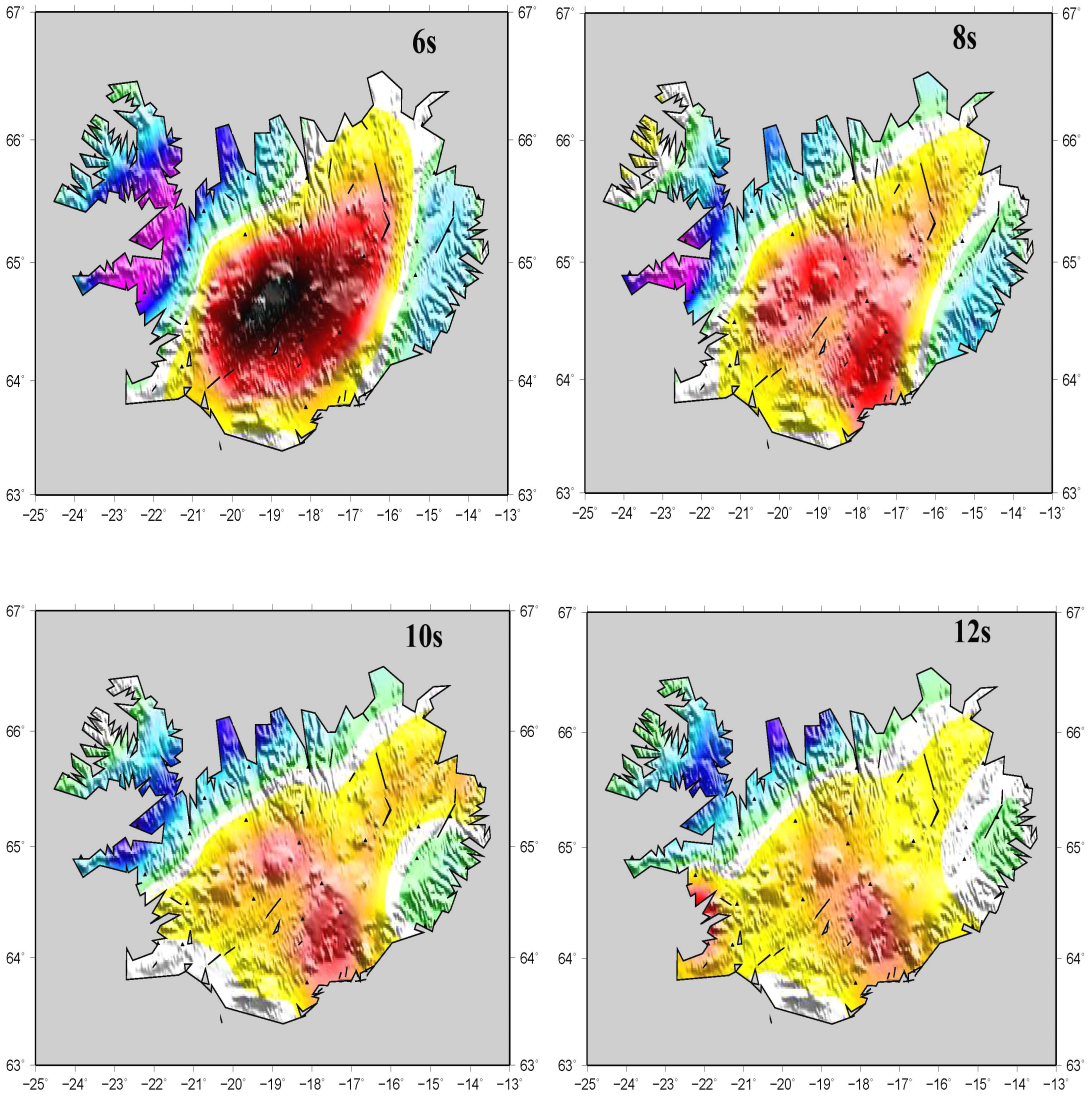

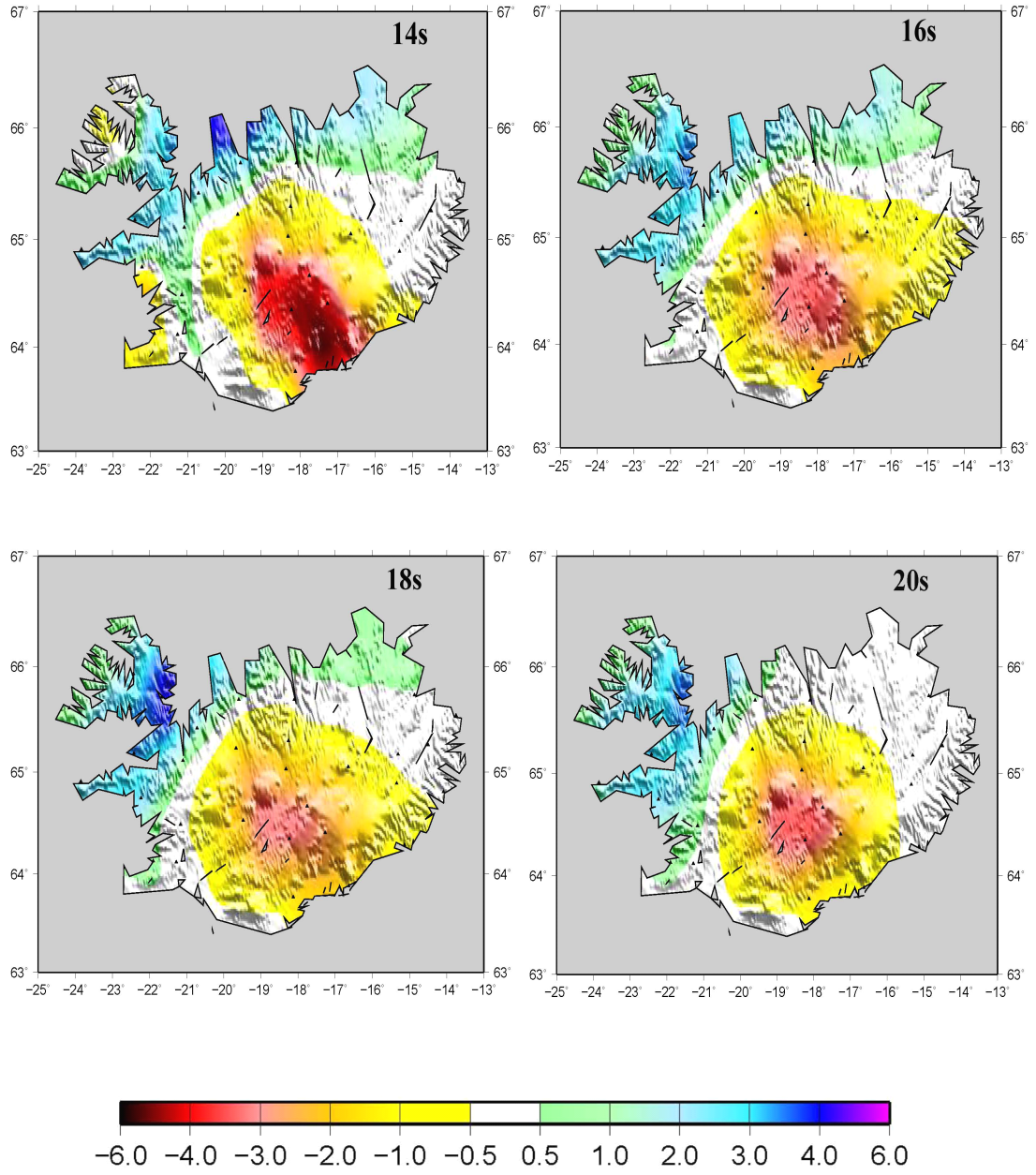

Figure 23 *Love wave Phase velocity tomography maps from Ambient Seismic Noise data from the HOTSPOT experiment in Iceland [1996 to 1998]. These are velocity anomaly maps and they illustrate the percentage velocity anomaly compared to local average velocities. The low velocity regions [in red, pink, orange] agree with the location of the expected active mid-ocean ridge in Iceland, with molten high temperature material that would cause these results.*

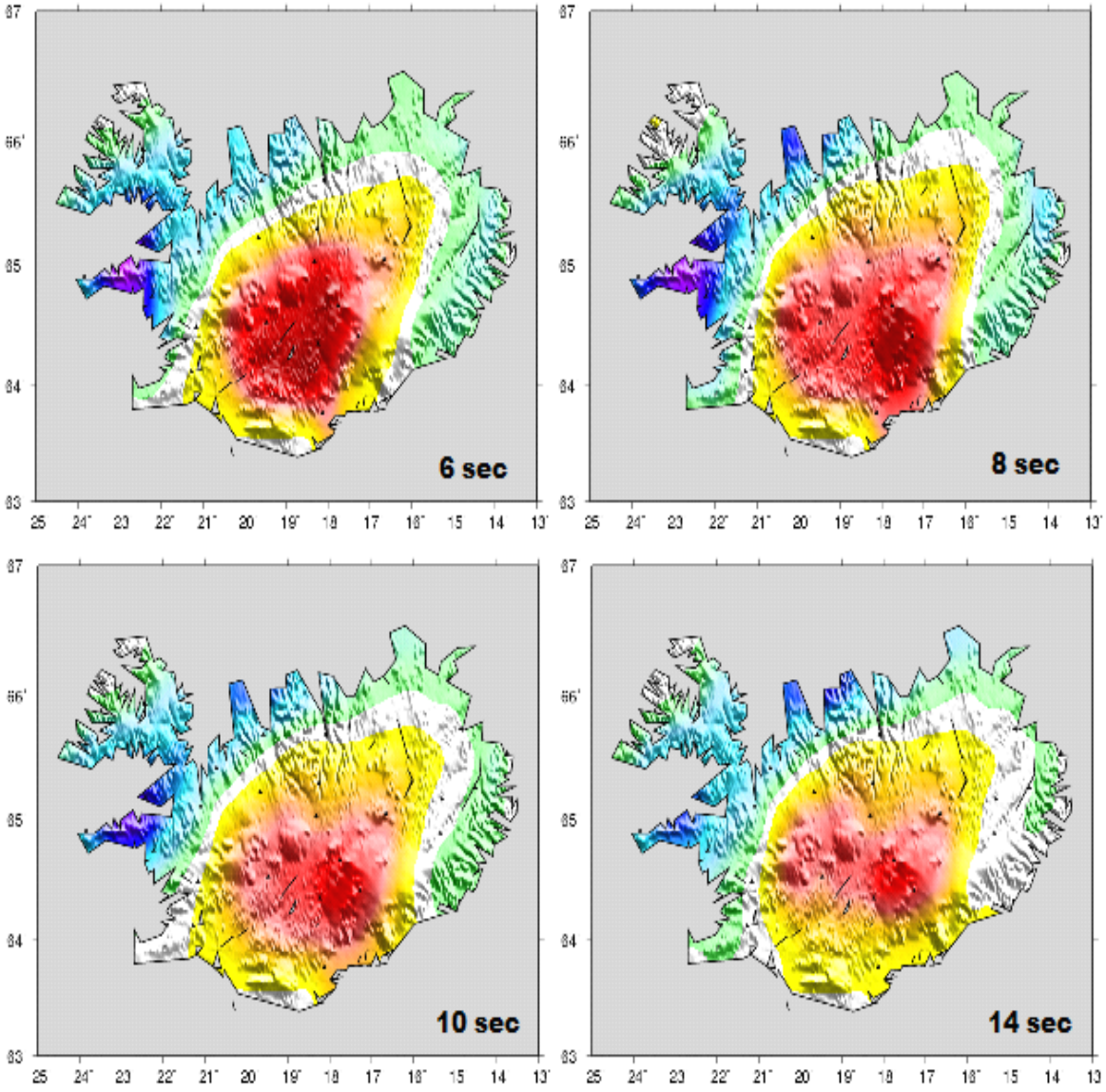
6 sec
8 sec
10 sec
14 sec

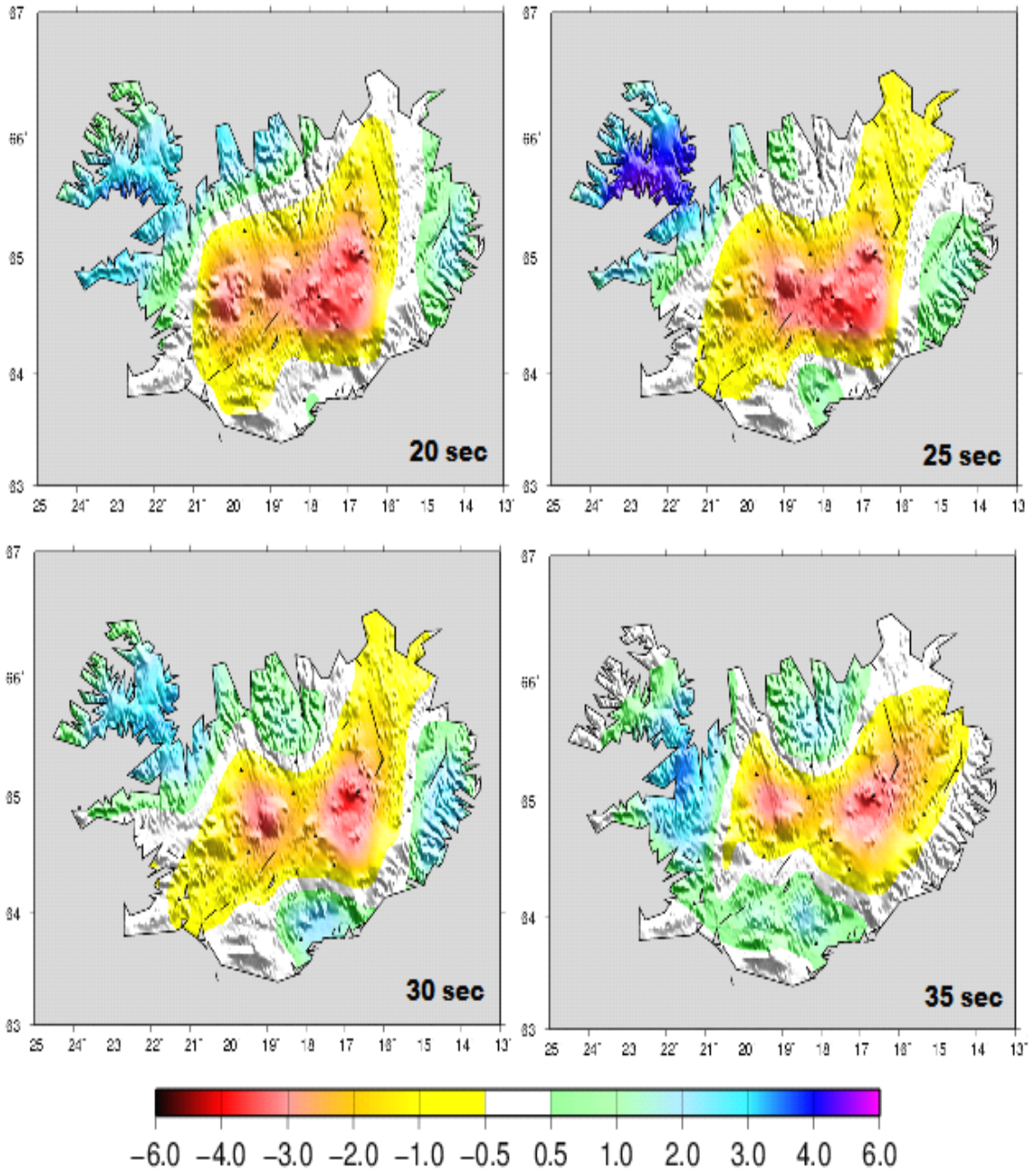

Figure 24 *Love wave Phase velocity tomography maps from Ambient Seismic Noise data from the HOTSPOT experiment in Iceland [1996 to 1998]. [Azevedo et al., 2012]*

Chapter 5 Shear-wave velocity

5.1 1-D isotropic inversion results

Although some conclusions can be drawn from surface-wave phase velocity anomaly maps shown in last chapter, but the interpretations based on them are not very accurate because each period of wave has a large range of sensitivity depth to the earth.. It is therefore necessary to invert Love wave phase velocities to obtain 1D and 3D shear-wave velocity structure of Icelandic crust.

Love wave phase velocities are inverted to isotropic shear-wave velocity using the method of Saito [1988]. The starting shear-wave velocity model used here is the AK135 global model that has been modified using the 1-D model of Iceland from Li and Detrick [2006]. Although Love wave phase velocity is not sensitive to P-wave velocity, we use a Vp/Vs ratio study by Allen *et al.* [2002]. In his research, he found a good correlation between P-wave and S-wave velocity of Vp/Vs ration starting form 1.78 with a slight gradient of 0.004 km^{-1}. It is not constant ratio in Icelandic crust. His conclusion is very important to estimate P-wave velocity in Iceland that is a significant parameter to input in this method.

The inversion from surface wave dispersion to shear-wave structure is a highly non-linear inverse problem [Dunkin, 1965]. The 1-D isotropic inversion in this study is a linearized inversion of a non-linear problem.

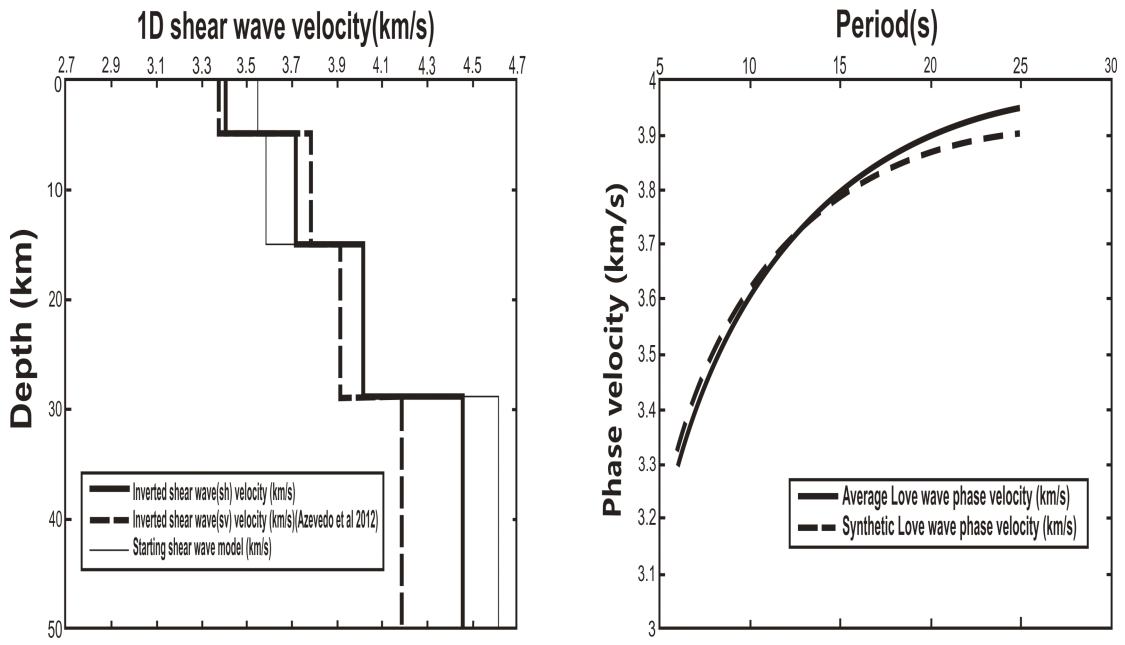

Figure 24 *(a) 1D shear-wave velocity model of Iceland. Solid line comes from inversion of Love wave phase velocity. Dash line represents shear wave velocity from Rayleigh wave inversion [Azevedo et al., 2012] and thin solid line is starting shear-wave model. (b) correlation between synthetic and observed Love wave phase velocity*

In this 1-D isotropic inversion, the crust in Iceland is divided into three layers: 0km-5km, 5km-15km, and 15km-29km. Here 29km is the average crustal thickness in Iceland based on the study of Allen *et al.* [2002]. Average phase velocities at different periods are used in the inversion for the 1-D average shear-wave model beneath Iceland. The method of Saito [1988] is used to compute the synthetic phase velocities and partial derivatives with respect to changes in *S*-wave speeds. The obtained 1-D shear-wave velocity model from Love wave dispersions are plotted in

Figure 24(a) and the corresponding synthetic and real average Love wave phase velocities are shown in Figure 24(b).

The thin solid line in Figure 24(a) is the starting AK135 shear-velocity model. The thick solid line in represents the shear-wave velocity model inverted from Love wave. The upper 5 km of the crust has an average SH shear-wave velocity of 3.41 km/s. The velocity increases to 3.72 km/s in the mid crust from 5 to 15 km and to 4.02 km/s in the lower crust. The predicted phase velocities from the 1D model can fit Love wave average phase velocities measurements satisfactorily. The data misfit increases at longer periods due to large errors in long period measurements. The dashed line in figure 24 (a) is the 1D Sv shear-wave velocity from Rayleigh wave constraints [Azevedo *et al.*, 2012]. Vsv changes from 3.38 km/s in the shallow crust to 3.79 km/s in the mid crust and to 3.92 km/s in the lower crust. There are differences between the 1D Vsv and Vsh model in Iceland. In the first layer, Vsh and Vsv are almost the same with Vsh slightly higher than Vsv while Vsh is significantly larger than Vsv in the lower crust. On the contrary, Vsh is smaller than Vsv in the mid crust. The incompatibilities between V_{SV} from Rayleigh wave and V_{SH} from Love wave indicates the presence of radial anisotropy, which is discussed in more detail in chapter 6.

5.2 3-D isotropic inversion results

The isotropic 3D model of SH-wave from Love wave dispersions is constructed by assembling the 1-D models at each 0.5° *0.5° map point with the same starting model. Then the inversion results of each grid are interpolated into 0.1° *0.1° grid points to get final inversion results. For the 3-D isotropic inversion, crustal thickness of every map point is an important parameter in the starting model.

In this study, crustal thickness is based on previous studies from Wide-Angle Experiments (Table 1) and receiver function analyses (Table 2). Then the point control crust thickness is interpolated to the whole study area (Figure 25). Figure 26 shows the 3D shear-wave perturbation maps. As in the 1D inversion, we divided the whole crust of Iceland into three layers. The first layer, 0-5km represents upper crust and the second layer, 5-15 km, can be considered as middle crust. The low crust, in this study, is represented by the third layer from 15km to the Moho. Low shear velocity anomalies, up to -6%, in the shallow and middle crust have an oval shape and are centered in central Iceland, concentrating on the MVZ and the north part of the WVZ and EVZ. This is expected due to partial melt and high temperature caused by ridges and mantle plume in Iceland. It is noticeable that the very northern part of low velocity anomaly in northern Iceland does not correspond with rift zone exactly in the upper crust and it moves further eastward in the middle crust. These features are not found in the results of 3D shear wave inversion from Rayleigh waves

(Figure 27). Given that the ray path coverage is poor in northeastern Iceland, the offset between the slow anomaly and the NVZ in northeastern Iceland is probably due to smearing along ray paths in that direction. In the deeper crust, the lowest velocity region is imaged as a much smaller anomaly, focused in a single circular area in southeast Iceland, right beneath the present location of the Iceland's hotspot. The overall slow anomaly in central Iceland in the lower crust is about -1%, significantly weaker than that in the middle and shallow crust. In northwest Iceland, both upper and lower crust are marked by high velocity anomaly. Relative cold crust, due to its location which is far away from rift zones, results this kind of anomaly.

Latitude	Longitude	Crustal thickness,km
66.17	-20.1	25.5
65.74	-19.6	28.3
65.36	-19.2	34.4
65.05	-18.4	41.7
64.86	-17.6	43.3
64.54	-16.8	42.2
65.87	-17.5	24.7
65.71	-16.8	19.4
65.56	-16.1	27.8
65.28	-15.5	35.0
65.09	-14.8	35.0
64.48	-22.1	23.2
64.14	-21.0	22.3
63.79	-19.9	21.2
63.95	-21.4	17.0
63.89	-22.2	15.2
63.81	-23.1	13.7
63.61	-23.5	14.0
63.33	-24.0	13.3
63.10	-24.5	12.7
63.03	-23.7	10.1
65.50	-17.5	25.5
65.30	-17.3	31.5

Table 1 *Point constrains on the depth of crust. [Darbyshire et al., 1998,Staple et al., 1997, Weir et al., 2001,Menke et al., 1998]*

Latitude	Longitude	Crustal Thickness, km
65.705	-21.678	25.7
65.598	-22.510	25.7
65.610	-24.161	25.0
65.874	-23.487	24.0
65.927	-22.428	23.7
64.749	-21.326	25.6
64.872	-19.559	30.5
64.560	-18.386	37.0
65.647	-16.915	20.5
66.077	-16.351	27.5
65.918	-17.578	21.0
66.133	-18.915	27.5
66.542	-18.010	16.0

Table 2 *Point constraints on the depth of crust. [Du and Foulger., 1999, Darbyshire et al., 2000]*

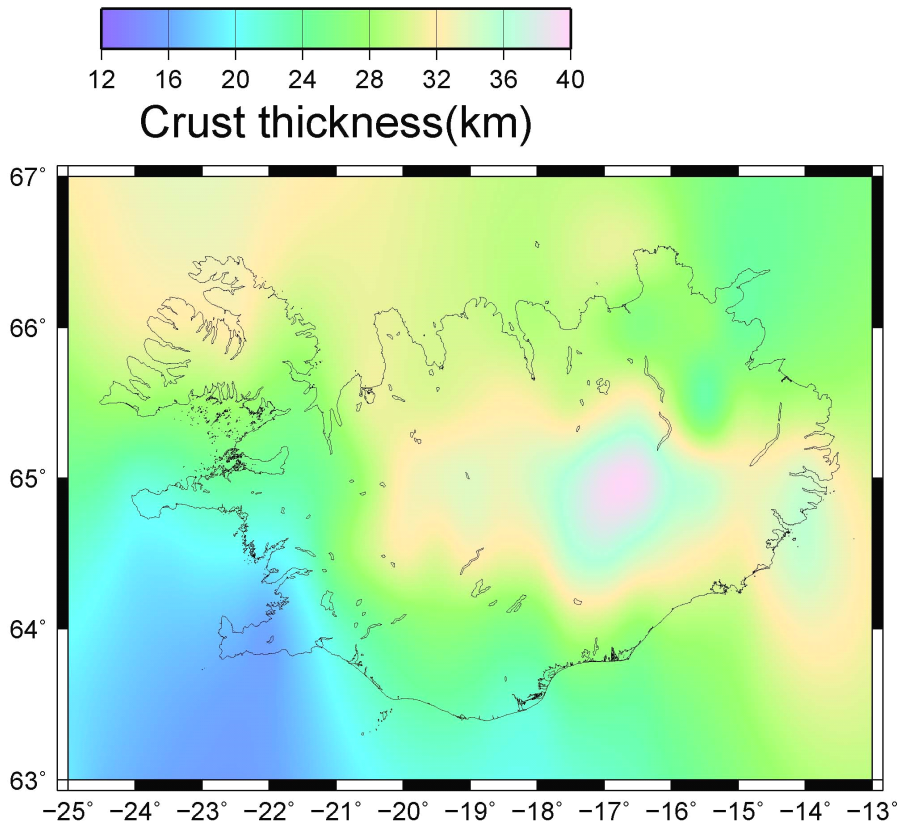

Figure 25 *Crustal thickness map from interpolation of Table 1 and Table2 in Km.*

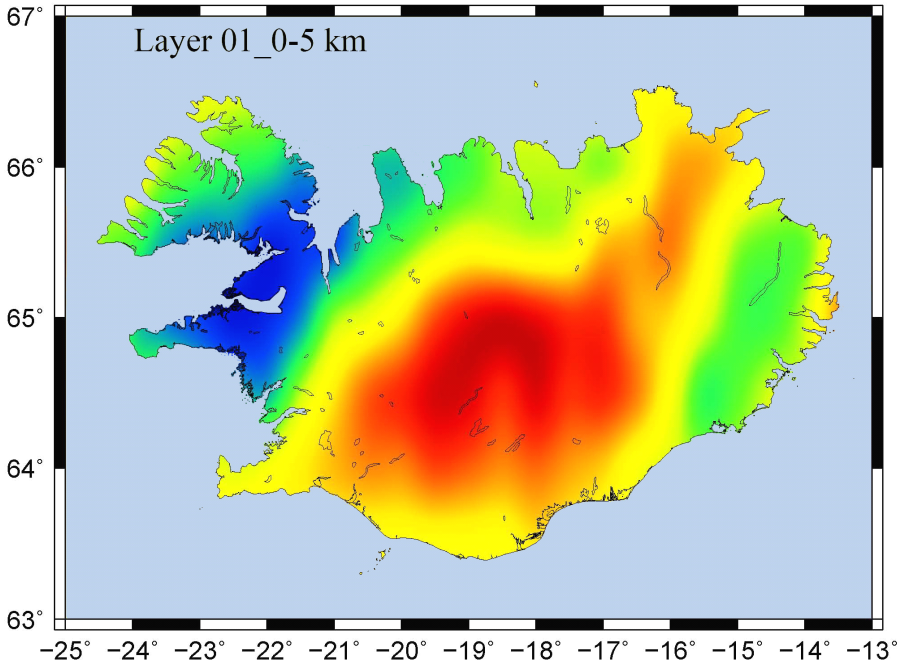
Layer 01_0-5 km
67°
66°
65°
64°
63°
−25° −24° −23° −22° −21° −20° −19° −18° −17° −16° −15° −14° −13°

(a)

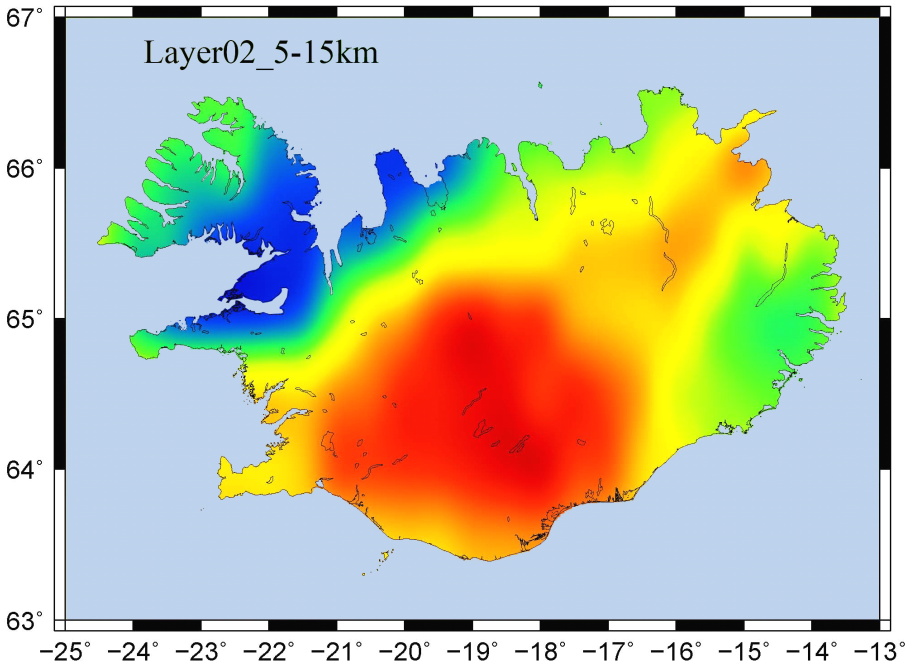
Layer02_5-15km
67°
66°
65°
64°
63°
−25° −24° −23° −22° −21° −20° −19° −18° −17° −16° −15° −14° −13°

(b)

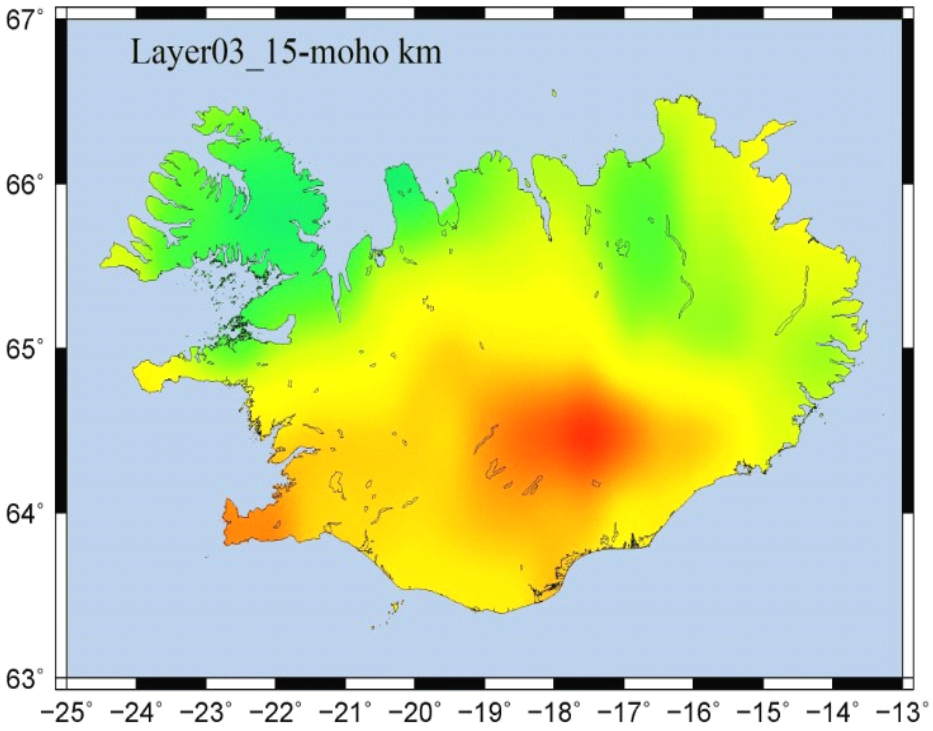

(c)

Figure 26 *Maps of shear wave anomalies at three layers in the crust of Iceland. a] Map of the shallow crust, up to 5 Km [b]Map of the mid crust, from 5 to 15Km and [c] Map of the deep crust from 15 Km to the Moho.*

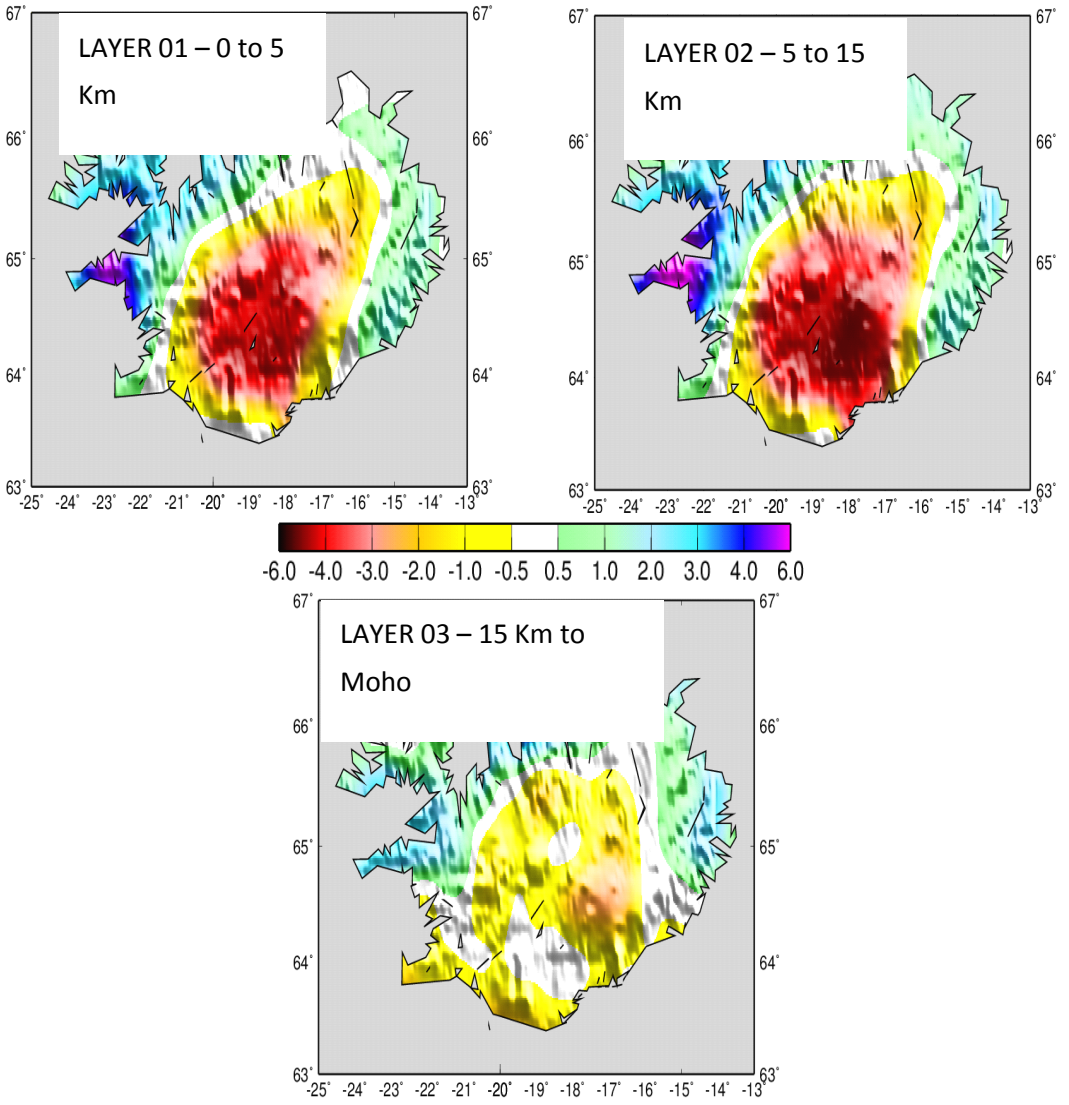

Figure 27 *3-D Shear Wave velocity anomaly map from Iceland's crust in percentage from ASN and teleseimic data recorded on the HOTSPOT network. [a] Map of the shallow crust, up to 5 Km [b]Map of the mid crust, from 5 to 15Km and [c] Map of the deep crust from 15 Km to the Moho.*

Chapter 6 Radial anisotropy in the crust

6.1 Introduction

Anisotropy can be defined as the variation of material's property with respect to the direction in which it is measured. It can exist in many scales from a mineral crystal to the whole global. Because the data used here are seismic data which are controlled by elastic properties of a rock, seismic anisotropy is to describe the directional dependence of seismic velocity in a rock. There are mainly two kinds of anisotropy. The first is that of transverse isotropy in which the elastic properties differ between the horizontal and vertical orientations [Anderson, 1961]. This type of anisotropy can be inferred from the incompatibilities between vertically polarized shear-wave (SV-waves) from Rayleigh wave and horizontally polarized shear-wave (SH-waves) from Love wave. The other type of anisotropy is azimuthal anisotropy, which can be observed from Rayleigh wave dispersion data [Forsyth, 1975]. This study will focus on radial anisotropy in Iceland.

Radially anisotropic shear-velocity structures are considered as a proxy for strain in the crust and mantle and are therefore of great interest to the earth science community. Crustal radial anisotropy model is very helpful to identify large-scale deformation and alignment of cracks and melt. For example, Moschetti *et al.* [2010] used the Rayleigh and Love waves from ambient noise tomography to build anisotropic crustal model (Figure 26) in the western United States. They observed

strong radial anisotropy with Vsh>Vsv in the lower crust that supports widespread lower crustal deformation in response to extension in the western United States.

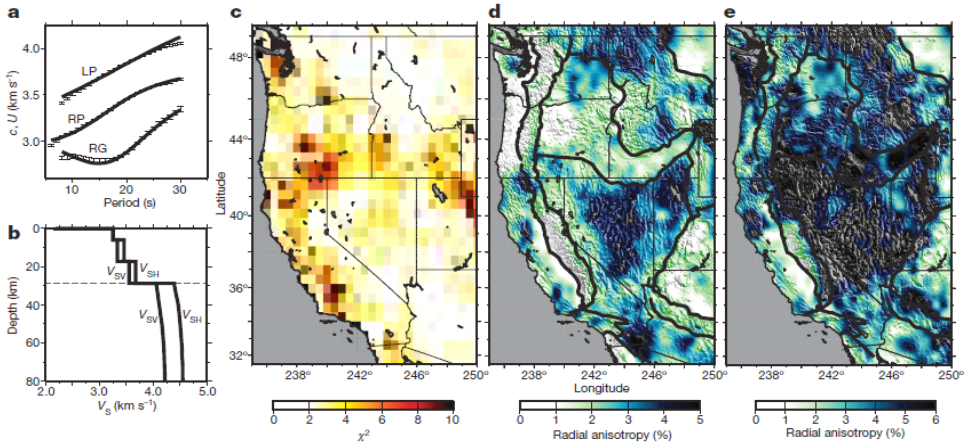

Figure 27 *Data mis-fit and the amplitude of radial anisotropy in the crust and upper mantle. [M.P.Moschetti et al ., 2010]*

6.2 Radial anisotropy model

Radial anisotropy is characterized by different elastic properties of a medium between the horizontal and vertical orientations. The property of an anisotropic medium can be represented by five independent components (C11, C12, C13, C33, and C44) and density. Radial anisotropy is marked by the difference between Vsh and Vsv. According to Fu and Li [2012], the best starting anisotropic model is a combination of the two isotropic models, which are velocity of horizontally polarized shear-wave (Vsh) model derived from Love wave inversion and velocity of vertically polarized shear-wave (Vsv) model derived from Rayleigh wave inversion. In 2010, Moschetti *et al.* demonstrated a new method to quantify the intense of radial

anisotropy. In his study, amplitudes of radial anisotropy is defined by the equation below:

$$2(V_{SH} - V_{SV}) / (V_{SH} + V_{SV})$$

Followed his method, combined with vertically polarized shear-wave velocity from Azvedo *et al.* [2012], I calculated the intense of radial anisotropy in upper crust and lower crust of whole Iceland in every imaging grid ($0.5^\circ * 0.5^\circ$). Then these relatively large image grids are interpolated to small image grid to increase the resolution. My final results are shown is figure 27.

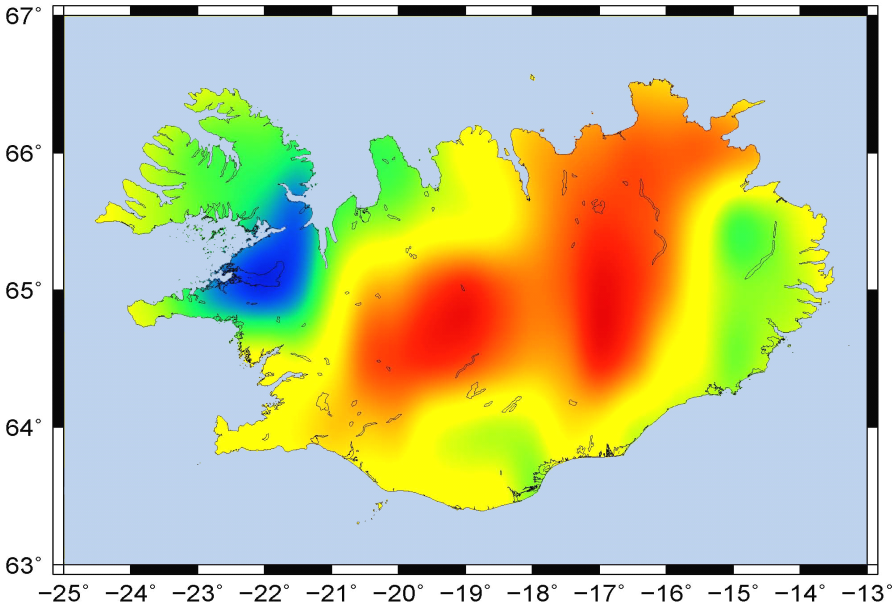

(a)

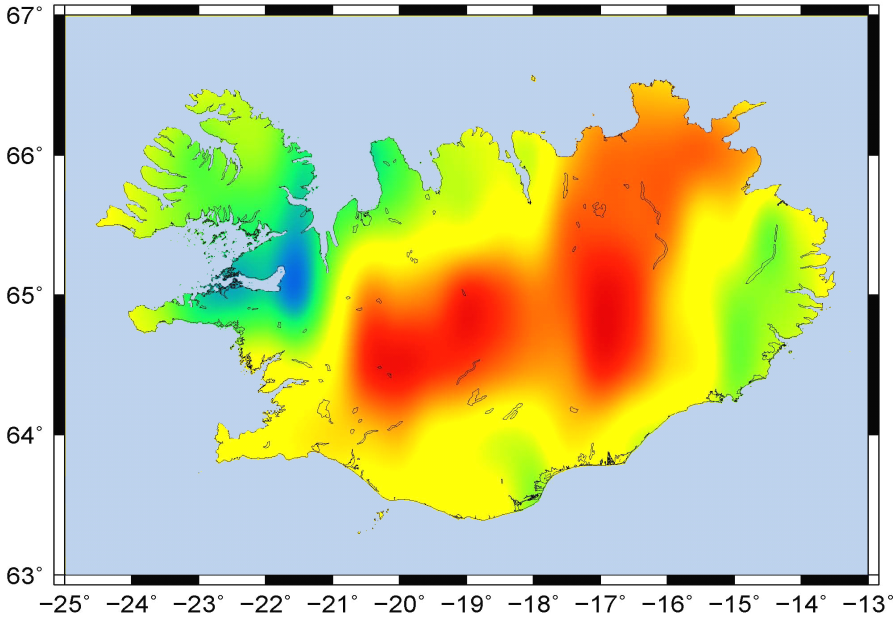

(b)

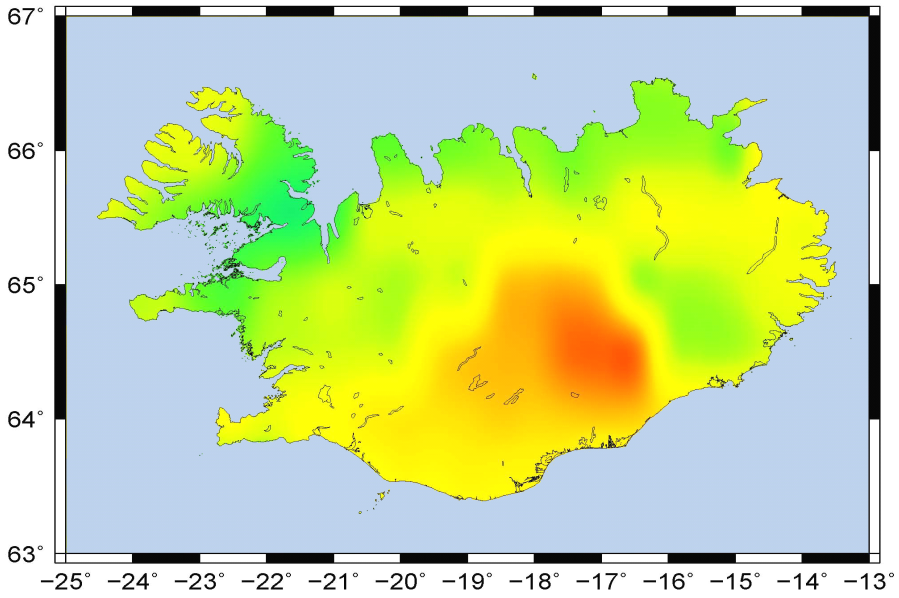

(c)

Figure 27 *Amplitude of radial anisotropy of upper crust(a), middle crust(b) and low crust(b).*

Yale and Sprunt [1989] proposed that a set of parallel fractures polarize shear waves. The polarization of one wave with faster velocity is parallel to the fracture strike and the other slower one has the polarization perpendicular to the fracture strike. This theory is based on lab measurement but can also be used to crustal scale structure. If Vsv is smaller than Vsh, it could indicate horizontal alignment of crustal materials and thin melt pockets due to plate spreading or horizontal magma flow while bigger Vsv may reflect vertical cracks and melt sills or sheeted dike complexes.

In the upper and middle crust of Iceland, the largest negative radial anisotropy, -6.0%, is found in Krafla, an active volcano. And the shape of this negative anisotropy is extremely similar to the ridges existing in Iceland. However, no obvious negative radial anisotropy is found in Eastern Volcanic Zone especially Hekla, the most active volcano from previous studies. This maybe caused by less dense ray path of this area. In lowe crust, only the region of mantle plume is marked by positive anisotropy and large area of rift zones have weak negative anisotropy. In addition, strong positive anisotropy appears in eastern and western coast which is far from ridges in both upper and lower crust. This can be explained as that the extensional deformation caused crustal minerals to align sub-horizontally.

CHAPTER 7 Discussion and conclusion

7.1 Discussion

The most remarkable characteristic of the 3-D crustal model in Iceland is the great slow anomaly in the upper and middle crust (0 to 15 km) in the central part of Iceland. This area consists of the Eastern and Middle Volcanic Zones and some active volcanoes, including Fogrufjoll, Grimsvotn, Vatnafjoll, Bardarbunfa, and Hofsjokull. These low velocities are likely to be a result of rock faulting and fracturing as well as high temperatures and partial melting. Individual magma chamber beneath the active volcanoes can't be resolved from the surface wave model due to the broad wavelength of 20 to 120 km for Rayleigh and Love waves from 5 to 30s. The broad low velocity anomaly is largely contributed by melt accumulation beneath the volcanoes and the rift zone.

Strong negative radial anisotropy (Vsv>Vsh) is found in central and northern Iceland. The shape of this negative radial anisotropy is extremely similar to the ridges existing in Iceland. The entire Northern, Western, and Middle Volcanic Zones are underlain by this kind of anisotropy. The lack of this anisotropy in southern Iceland is more likely due to poor resolution from the data. The negative radial anisotropy beneath the rift zones can be caused by sheeted dikes, vertical alignment of cracks, and vertical magma flow or melt sills.

Allen *et al* in 2002 proposed that a plume-driven plumbing system in Iceland crust, where magma is fed from the core of the mantle plume vertically up through the lower crust in central Iceland and then laterally along the upper crustal rift system. However, no evidence has been found in this study to support lateral crustal flow along the rift zones in the upper crust of Iceland. If the hot magma from mantle plume feed the rift system horizontally, positive anisotropy (Vsh>Vsv) should be observed beneath the volcanic zones in the upper crust of Iceland.

No matter long periods Love and Rayleigh phase velocities anomaly maps or shear wave structure from inversion have a low velocity looked like a single, circle in MVZ and Bardarbunga-Grimsvotn volcanic complex. Bardabunga-Grimsvotn volcanic complex has been one of the most active complexes during the last 100 years and our extremely obvious low velocity anomaly can be interpreted as a plume. This interpretation has been supported by many previous studies [Tryggvason *et al*., 1983; Wolfe *et al*., 1997; Allen *et al*., 1999; Foulger *et al*., 2000; Allen *et al*., 2002]. This conclusion is also further supported by geochemistry study. High 3He/4He are classic signature of mantle plume. This feature has been largely found from erupted lava centered on Bardarbunga-Grimsvotn. This kind of plumb-like low velocity anomaly in the low crust of Iceland indicates the existence hot temperature and partial melt associated with the plume. Furthermore, This region is marked by negative radial anisotropy which means Vsv is larger than Vsh indicating the existence of vertical magma flow. Most importantly, large region of Iceland, especially some areas of rift

places in low crust are marked by positive anisotropy which means Vsh is larger than Vsv. In one hand, positive anisotropy areas which is away from rift zones indicates the existence of spreading force. In the other hand, positive anisotropy in rift zones suggests lateral horizontal flow in the lower crust of Iceland. This lateral horizontal flow indicates the ridge is fed by the plume source in the lower crust. Melt and magma produced by the plume is still the dominant mechanism for forming the Icelandic crust.

7.2 Conclusion

Ambient noise tomography method is successfully used to increase model resolution in Icelandic crust. Low velocity anomaly is largely found in central Iceland and along rift zones in shallow and middle crust. In the lower crust, low velocity present in the location of mantle plume. Fast anomalies are imaged in areas far away from rift zones, which seems to be formed by cooled down basalt.

These low velocities anomaly in shallow and middle crust can be interpreted as partial melt that feeds the local volcanoes and in the lower crust, the low velocities, near the projected hotspot, can indicate melt accumulation or high temperature from the Iceland plume.

A 3D radial anisotropy model is also established in Iceland. In the middle and shallow crust, large negative radial anisotropy covers central Iceland and along the rift zones which means partial melt from rifting is the dominate source of the low velocity

rather than fed by mantle plume which is revealed by positive radial anisotropy. In the lower crust, negative anisotropy which indicates the present of vertical pipes fluxing material supports plume like lower crust model. Furthermore, positive anisotropy in rift zones suggests lateral horizontal flow in the lower crust of Iceland. This lateral horizontal flow indicates the ridge is fed by the plume source in the lower crust. Melt and magma produced by the plume is still the dominate mechanism for forming the Icelandic crust.

REFERENCES

Allen, R. M., G. Nolet, W. J. Morgan, K. Vogfjord, B. H. Bergsson, P. Erlendsson, G. R. Foulger, S. Jakobsdottir, B. R. Julian, M. Pritchard, S. Ragnarsson, and R. Stefansson, (1999), The thin hot plume beneath Iceland*, Geophys. J. Int.,* 137, 51– 63.

Allen, R. M., G. Nolet, W. J. Morgan, K. Vogfjo¨rd, M. Nettles, G. Ekstrom, B. H. Bergsson, P. Erlendsson, G. R. Foulger, S. Jakobsdottir, B. R. Julian, M. Pritchard, S. Ragnarsson, and R. Stefansson, (2002), Plume-driven plumbing and crustal formation in Iceland, *J. Geophys. Res.*, 107(B8), 2163, doi:10.1029/2001JB000584.

Allen, R. M., Nolet, G., Morgan, W.J., Vogfjord, K, Bergsson, B.H.,Erlendsoon, P., Foulger,G. R., Jakobsdottir, S., Julian, B., Pritchard, M., and Ragnarsson, S., (2002b), Imaging the mantle beneath Iceland using integrated seismological techniques, *J. Geophys. Res.*, 107(B12), 2325, doi:10.1029/2001JB000595.

Bath, M., (1960), Crustal structure of Iceland, *J. geophys. Res.*, 65, 1793–1807.

Bensen, G. D., M. H. Ritzwoller, M. P. Barmin, A. L. Levshin, F. Lin, M. P. Moschetti, N. M. Shapiro, and Y. Yang, (2007), Processing seismic ambient noise data to obtain reliable broad-band surface wave dispersion measurements, *Geophys. J. Int.*, 169, 1239–1260.

Bjarnason, I. T., W. Menke, O . Flovenz, and D. Caress, (1993), Tomographic image of the Mid-Atlantic plate boundary in southwestern Iceland, *J. Geophys. Res.*, 98, 6607–6622.

Darbyshire, F. A., I. T. Bjarnason, R. S. White, and O. Flovenz, (1998), Crustal structure above the Iceland mantle plume imaged by the ICEMELT refraction profile, *Geophys. J. Int.*, 135, 1131– 1149.

Darbyshire, F. A., K. F. Priestley, R. S. White, R. Stefansson, G. B. Gudmundsson, and S. Jakobsdottir, (2000), Crustal structure of central and northern Iceland from analysis of teleseismic receiver functions, *Geophys. J. Int.*, 143, 163– 184.

Darbyshire, F. A., R. S. White, and K. F. Priestley, (2000b), Structure of the crust and uppermost mantle of Iceland from a combined seismic and gravity study, *Earth Planet. Sci. Lett.*, 181, 409– 428.

Du, Z., and Foulger, G.R., (1999), The crustal structure beneath the Northwest Fjords, Iceland, from receiver functions and surface waves. *Geophys. J. Int.* 139, 419– 432.

Du, Z.J., and Foulger G.R., (2001), Variation in the crustal structure across central Iceland. *Geophys. J. Int.* 145, 246– 264.

Du, Z., Foulger, G.R., Julian, B.R., Allen, R.M., Nolet, G., Morgan, W.J., Bergsson, B.H., Erlendsson, P., Jakobsdottir, S., Ragnarsson, S., Stefansson, R., and Vogfjord, K., (2002), Crustal structure beneath western and eastern Iceland from surface waves and receiver functions. *Geophys. J. Int.* 149, 349–363.

Einarsson, T., (1957), Magneto-geological mapping in Iceland with the use of a compass. *Adv. Phys.*, 6, 232-239.

Einarsson, P., Bjornsson, S., (1979), Earthquakes in Iceland. *Jokull,* 29, 37-43.

Einarsson, P., B. Brandsdottir, M. T. Gudmundsson, H. Bjornsson, K., Gronvold, and F. Sigmundsson, (1997), Center of the Iceland hotspot experiences volcanic unrest, *Eos Trans. AGU*, 78, 369, 374–375.

Eysteinsson, H. & Gunnarsson, K., (1995), Maps of gravity, bathymetry and magnetics for Iceland and surroundings, *National Energy Authority*, Reykjavik.

Fedorova, T., Jacoby, W.R., Wallner, H., (2005), Crust–mantle transition and Moho model for Iceland and surroundings from seismic, topography, and gravity data. *Tectonophysics*, 396, 119-140.

Flovenz, O.G., (1980), Seismic structure of the Icelandic crust above layer three and the relation between body wave velocity and the alteration of the basaltic crust*, J. Geophys*., 47, 211–220.

Flovenz, O., and K. Gunnarsson, (1991), Seismic crustal structure in Iceland and surrounding area, *Tectonophysics*, 189, 1– 17.

Flovenz, O.G. & Saemundsson, K., (1993), Heat flow and geothermal processes in Iceland, *Tectonophysics*, 225, 123–138.

Foulger, G.R. and Pearson, D.G., (2001), Is Iceland underlain by a plume in the lower mantle? Seismology and helium isotopes, *Geophys. J. Int.,* 145**,** F1–F5.

Foulger, G.R., (2002), Plumes, or plate tectonic processes?, *Astron. Geophys*., 43, 6.19–6.23.

Foulger, G.R., (2003), On the apparent eastward migration of the spreading ridge in Iceland, abstract in *The Hotspot Handbook, Proceedings of Penrose Conference Plume IV: Beyond the Plume Hypothesis*, Hveragerdi, Iceland, 25-28.

Foulger, G.R., Pritchard, M.J., Julian, B.R., Evans, J.R., Allen, R.M., Nolet, G., Morgan, W.J., Bergsson, B.H., Erlendsson, P., Jakobsdottir, S., Ragnarsson, S., Stefansson, R., and Vogfjord, K., (2001), Seismic tomography shows that upwelling beneath Iceland is confined to the upper mantle. *Geophys. J. Int.* 146, 504–530.

Foulger, G.R., (2002), Plumes, or plate tectonic processes?, *Astron. Geophys.*, 43, 6.19–6.23.

Foulger, G.R., Du, Z., and Julian, B.R., (2003), Icelandic-type crust. *Geophys. J. Int.* 155, 567–590.

Foulger, G.R. et al., (2000), The seismic anomaly beneath Iceland extends down to the mantle transition zone and no deeper, *Geophys. J. Int.*, 142, F1–F5.

Fowler, C.M.R., (1976), Crustal structure of the mid-Atlantic ridge crest at 37◦N, *Geophys. J. R. Astr. Soc.*, 47, 459–491.

Fowler, C.M.R., (1978), The mid-Atlantic ridge: structure at 45◦N, *Geophys. J. R. Astr. Soc.*, 54, 167–183.

Gebrande, H., Miller, H. & Einarsson, P., (1980), Seismic structure of Iceland along RRISP-Profile I, *J. Geophys.*, 47, 239–249.

Gudmundsson, O., (2003), The dense root of the Iceland crust. *Earth and Planet. Sci. Lett.* 206, 427-440.

Gudmundsson, O., Khan, A. and Voss, P., (2007), Rayleigh-wave group-velocity of the icelandic crust from correlation of ambient seismic noise, *Geophys. Res. Lett.*, 34, L14314, doi:10.1029/2007GL030215.

Jones, S.M., Maclennan, J., (2005), Crustal Flow beneath Iceland, *J. Geophysical Research*, 110, B09410, doi:10.1029/2004JB003592.

Kaban, M. K., Flovenz, O., Palmason, G., (2002), Nature of the crust-mantle transition zone and the thermal state of the upper mantle beneath Icealand from gravity modeling, *Geophys. J. Int.*149, 281–299.

Kristjánsson, L. and G. Jónsson., (1998), Aeromagnetic results and the presence of extinct rift zone in Western Iceland, *J.Geodyn.25, 99-108.*

Kristjánsson, L. (2002), Estimating properties of the geomagnetic field from Icelandic lavas. *Phys. Chem. Earth* 27, 1205–1213.

Kristjánsson, L. and G. Jónsson (2007), Paleomagnetism and magnetic anomalies in Iceland. *J. Geodyn.* 43, 30–54.

Li, A., and R. Detrick, (2003), Azimuthal anisotropy and phase velocity beneath Iceland: implication for plume-ridge interaction, *Earth Planet. Sci. Lett.*, 214, 1-2, 153-165.

Li, A. and R.S. Detrick, (2006), Seismic structure of Iceland from Rayleigh wave inversions and geodynamic implications, *Earth Planet. Sci. Lett.*, 241, 901-912.

Menke, W., (1999), Crustal isostasy indicates anomalous densities beneath Iceland, *Geophys. Res. Lett.*, 26, 1215–1218.

Menke, W. & Levin, V., (1994), Cold crust in a hot spot, *Geophys. Res. Lett.*, 21, 1967–1970.

Menke,W. & Sparks, D., (1995), Crustal accretion model for Iceland predicts 'cold' crust, *Geophys. Res. Lett.*, 22, 1673–1676.

M.P.Moschetti, M.H.Ritzwoller, F.Lin & Y. Yang., (2010), Seismic evidence for widespread western-US deep-crustal deformation caused by extension, *Nature,* 464, doi:10.1038.

Palmason, G., (1971), Crustal Structure of Iceland from Explosion Seismology, *Soc. Sci. Isl.*, XL.

Palmason, G., (1974), Heat flow and hydrothermal activity in Iceland, *Geodynamic of Iceland and the N. Atlantic area*, pp. 297–306, ed. Kristjansson, L., Reidel, Dordrecht.

Palmason, G., (1980), A continuum model of crustal generation in Iceland; kinematic aspects, *J. Geophys.*, 47, 7–18.

Saemundsson, K., (1979), Outline of the geology of Iceland*, Jokull*, 29, 7–28.

Saemundsson, K., Kristjansson, L., McDougall, I. & Watkins, N.D., (1980), K-Ar dating, geological and paleomagnetic study of a 5-km lava succession in northern Iceland, *J. geophys. Res.*, 85, 3628–3646.

Saito, M., (1988), DISPER80: a subroutine package for the calculation of seismic normal-mode solutions, in *Seismological Algorithms*, pp. 293– 319, ed. D.J. Doornbos, Elsevier, New York.

Shapiro, N. M., and M. Campillo, (2004), Emergence of broadband Rayleigh waves from correlations of the ambient seismic noise, *Geophys. Res. Lett.*, 31, L07614.

Shapiro, N. M., M. Campillo, L. Stehly, and M. H. Ritzwoller, (2005), High resolution surface-wave tomography from ambient seismic noise, *Science*, 307, 1615–1618.

Staples, R.K., (1997), Crustal structure above the Iceland mantle plume, PhD thesis, *University of Cambridge*, Cambridge.

Tryggvason, E., (1962), Crustal structure of the Iceland region from dispersion of surface waves, *Bull. Seism. Soc. Am.*, 52, 359–388.

Tryggvason, E., (1964), Arrival times of P waves and upper mantle structure, *Bull. Seism. Soc. Am.*, 54, 727–736.

Weir, N.R.W., White, R.S., Brandsdottir, B., Einarsson, P., Shimamura, H. & Shiobara, H., (2001), Crustal structure of the northern Reykjanes ridge and Reykjanes peninsula, southwest Iceland*, J. Geophys. Res.*, 106, 6347– 6368.

Yale, D.P. and Sprunt,E.S., (1989), Prediction of fracture direction using shear acoustic anisotropy, *Log Analyst.*, March-April,65-70.

Yang, Y., M. H. Ritzwoller, A. L. Levshin, and N. M. Shapiro, (2007), Ambient noise Rayleigh wave tomography across Europe, *Geophys. J. Int.*, 168[1], 259– 274

Yang, Y., and M. H. Ritzwoller, (2008), The characteristics of ambient seismic noise as a source for surface wave tomography, *Geochem. Geophys. Geosyst.*, 9, Q02008.

Yang, Y., Li, A., and Ritzwoller, M.H., (2008), Crustal and uppermost mantle structure in southern Africa revealed from ambient noise and teleseismic tomography, *Geophys. J. Int.*, 174, 235–248.